

One-Pass Error Bounded Trajectory Simplification

Xuelian Lin Shuai Ma Han Zhang Tianyu Wo Jinpeng Huai

SKLSDE Lab, Beihang University, Beijing, China

Beijing Advanced Innovation Center for Big Data and Brain Computing, Beijing, China

{linxl, mashuai, zhanghan, woty, huaijp}@buaa.edu.cn

ABSTRACT

Nowadays, various sensors are collecting, storing and transmitting tremendous trajectory data, and it is known that raw trajectory data seriously wastes the storage, network band and computing resource. Line simplification (LS) algorithms are an effective approach to attacking this issue by compressing data points in a trajectory to a set of continuous line segments, and are commonly used in practice. However, existing LS algorithms are not sufficient for the needs of sensors in mobile devices. In this study, we first develop a one-pass error bounded trajectory simplification algorithm (OPERB), which scans each data point in a trajectory once and only once. We then propose an aggressive one-pass error bounded trajectory simplification algorithm (OPERB-A), which allows interpolating new data points into a trajectory under certain conditions. Finally, we experimentally verify that our approaches (OPERB and OPERB-A) are both efficient and effective, using four real-life trajectory datasets.

1. INTRODUCTION

Various mobile devices, such as smart-phones, on-board diagnostics, personal navigation devices, and wearable smart devices, have been widely using their sensors to collect massive trajectory data of moving objects at a certain sampling rate (*e.g.*, 5 seconds), and transmit it to cloud servers for location based services, trajectory mining and many other applications. It is known that transmitting and storing raw trajectory data consumes too much network bandwidth and storage capacity [2–4, 10–13, 15, 18–22]. Further, we find that the online transmitting of raw trajectories also seriously aggravates several other issues such as out-of-order and duplicate data points in our experiences when implementing an online vehicle-to-cloud data transmission system. Fortunately, these issues can be resolved or greatly alleviated by the trajectory compression techniques [2–4, 6, 8, 11–13, 15, 18, 19, 21, 23, 24], among which line simplification based methods are widely used [2–4, 6, 8, 11, 12, 18, 23], due to their distinct advantages: (a)

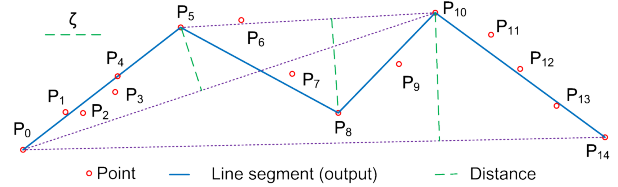


Figure 1: A trajectory $\tilde{\gamma}[P_0, \dots, P_{14}]$ with fifteen points is represented by four continuous line segments (solid blue), compressed by the Douglas–Peucker algorithm [6].

simple and easy to implement, (b) no need of extra knowledge and suitable for freely moving objects [20], and (c) bounded errors with good compression ratios. Line simplification algorithms belong to lossy compression, and use a set of continuous line segments to represent a compressed trajectory, as shown in Figure 1.

The most notable line simplification (LS) algorithm is the Douglas-Peucker algorithm [6] invented in 1970s, for reducing the number of points required to represent a digitized line or its caricature in the context of computer graphics and image processing. The basic Douglas-Peucker algorithm (DP) is a batch method with a time complexity of $O(n^2)$, where n is the number of data points in a given trajectory to be compressed. Its batch nature and high time complexity make it not suitable for the online scenarios. Several LS algorithms have been developed based on DP, *e.g.*, by combining DP with sliding/open windows [11, 15] for online processing. However, these methods still have a high time and/or space complexity, which significantly hinders their utility in resource-constrained mobile devices [12].

Recently, BQS [12] has been proposed, using a new distance checking method by picking out at most eight special points from an open window based on a convex hull, *e.g.*, a rectangular bounding box with two bounding lines, so that when a new point is added to a window, it only needs to calculate the distances of the special points to a line, instead of all data points in the window, in many cases. The time complexity of BQS remains $O(n^2)$ in the worst case, as BQS falls back to DP when the eight special points cannot be used. However, its simplified version, FBQS directly outputs a line segment, and starts a new window when the eight special points cannot bound all the points considered so far. Indeed, FBQS has a linear time complexity, and is the fastest LS based solution for trajectory compression.

An LS algorithm is *one-pass* if it processes each point in a trajectory once and only once when compressing the trajectory. Obviously, one-pass algorithms have low time and space complexities, and are more appropriate for online pro-

This work is licensed under the Creative Commons Attribution-NonCommercial-NoDerivatives 4.0 International License. To view a copy of this license, visit <http://creativecommons.org/licenses/by-nc-nd/4.0/>. For any use beyond those covered by this license, obtain permission by emailing info@vldb.org.

Proceedings of the VLDB Endowment, Vol. 10, No. 3
Copyright 2016 VLDB Endowment 2150-8097/16/11.

cessing. Unfortunately, existing algorithms such as DP, BQS and FBQS are not one-pass, as data points in a trajectory are processed multiple times in these algorithms. Indeed, *it remains open whether there exist one-pass error bounded LS based effective trajectory compression algorithms.*

Contributions & Roadmap. To this end, we propose two one-pass error bounded LS based algorithms for compressing trajectories in an efficient and effective way.

(1) We first develop a one-pass error bounded trajectory simplification algorithm (OPERB, Section 3) that runs in $O(n)$ time and $O(1)$ space. OPERB is based on a novel local distance checking method, and equipped with five optimization techniques to further improve its compression ratio.

(2) We then propose an aggressive one-pass error bounded trajectory simplification algorithm (OPERB-A, Section 4) that remains in $O(n)$ time and $O(1)$ space. OPERB-A allows interpolating new data points into a trajectory under certain conditions and with practical considerations. The rationale lies in that moving objects have sudden track changes while data points may not be sampled due to various reasons.

(3) Using four real-life trajectory datasets (Taxi, Truck, SerCar, GeoLife), we finally conduct an extensive experimental study (Section 5), by comparing our algorithms OPERB and OPERB-A with FBQS (*the fastest* existing LS algorithm) and DP (*the best* existing LS algorithm in terms of *compression ratio*). We find that OPERB and OPERB-A are on average (4.1, 4.1, 5.4, 5.2) times faster than FBQS on (Taxi, Truck, SerCar, GeoLife), respectively. For compression ratios, OPERB is comparable with DP, and OPERB-A is better than DP that is on average (84.2%, 86.4%, 97.1%, 94.7%) of DP on (Taxi, Truck, SerCar, GeoLife), respectively.

All detailed proofs and extra analyses can be found in [1].

2. PRELIMINARIES

In this section, we introduce some basic concepts and existing algorithms for trajectory simplification.

2.1 Basic Notations

Points (P). A data point is defined as a triple $P(x, y, t)$, which represents that a moving object is located at *longitude* x and *latitude* y at *time* t . Note that data points can be viewed as points in a three-dimension Euclidean space.

Trajectories (\vec{T}). A trajectory $\vec{T}[P_0, \dots, P_n]$ is a sequence of data points in a monotonically increasing order of their associated time values (*i.e.*, $P_i.t < P_j.t$ for any $0 \leq i < j \leq n$). Intuitively, a trajectory is the path (or track) that a moving object follows through space as a function of time [16].

Directed line segments (\mathcal{L}). A directed line segment (or line segment for simplicity) \mathcal{L} is defined as $\overrightarrow{P_s P_e}$, which represents the closed line segment that connects the start point P_s and the end point P_e . Note that here P_s or P_e may not be a point in a trajectory \vec{T} , and hence, we also use notation \mathcal{R} instead of \mathcal{L} when both P_s and P_e belong to \vec{T} .

We also use $|\mathcal{L}|$ and $\mathcal{L}.\theta \in [0, 2\pi)$ to denote the length of a directed line segment \mathcal{L} , and its angle with the x -axis of the coordinate system (x, y) , where x and y are the longitude and latitude, respectively. That is, a directed line segment $\mathcal{L} = \overrightarrow{P_s P_e}$ can be treated as a triple $(P_s, |\mathcal{L}|, \mathcal{L}.\theta)$.

Piecewise line representation (\vec{T}). A piece-wise line representation of a trajectory $\vec{T}[P_0, \dots, P_n]$ is $\vec{T}[\mathcal{L}_0, \dots, \mathcal{L}_m]$

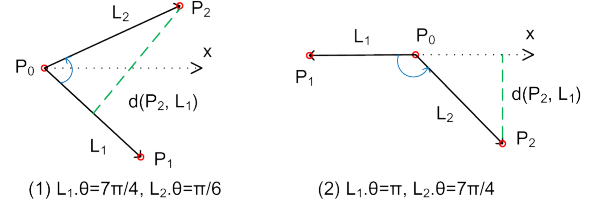


Figure 2: Example included angles and distances.

($0 < m \leq n$), a sequence of continuous directed line segments $\mathcal{L}_i = \overrightarrow{P_{s_i} P_{e_i}}$ of \vec{T} ($i \in [0, m]$) such that $\mathcal{L}_0.P_{s_0} = P_0$, $\mathcal{L}_m.P_{e_m} = P_n$ and $\mathcal{L}_i.P_{e_i} = \mathcal{L}_{i+1}.P_{s_{i+1}}$ for all $i \in [0, m-1]$. Note that each directed line segment in \vec{T} essentially represents a continuous sequence of data points in \vec{T} .

Included angles (\angle). Given two directed line segments $\mathcal{L}_1 = \overrightarrow{P_s P_{e_1}}$ and $\mathcal{L}_2 = \overrightarrow{P_s P_{e_2}}$ with the same start point P_s , the included angle from \mathcal{L}_1 to \mathcal{L}_2 , denoted as $\angle(\mathcal{L}_1, \mathcal{L}_2)$, is $\mathcal{L}_2.\theta - \mathcal{L}_1.\theta$. For convenience, we also represent the included angle $\angle(\mathcal{L}_1, \mathcal{L}_2)$ as $\angle P_{e_1} P_s P_{e_2}$.

Distances (d). Given a point P_i and a directed line segment $\mathcal{L} = \overrightarrow{P_s P_e}$, the distance of P_i to \mathcal{L} , denoted as $d(P_i, \mathcal{L})$, is the Euclidean distance from P_i to the line $\overrightarrow{P_s P_e}$, commonly adopted by most existing LS methods, *e.g.*, [3, 6, 8, 11, 12].

Example 1: (1) In Figure 1, the four continuous directed line segments $\overrightarrow{P_0 P_5}$, $\overrightarrow{P_5 P_8}$, $\overrightarrow{P_8 P_{10}}$, $\overrightarrow{P_{10} P_{14}}$ form a piecewise line representation of trajectory $\vec{T}[P_0, \dots, P_{14}]$.

(2) Figure 2 shows two different cases of included angles. In each case, there are two directed line segments $\mathcal{L}_1 = \overrightarrow{P_0 P_1}$ and $\mathcal{L}_2 = \overrightarrow{P_0 P_2}$ with the same start point P_0 . The included angle $\angle(\mathcal{L}_1, \mathcal{L}_2)$ from \mathcal{L}_1 to \mathcal{L}_2 lies in $(-2\pi, 2\pi)$, and is $\frac{-19\pi}{12}$ and $\frac{3\pi}{4}$ in Figures 2(1)&(2), respectively.

(3) The distance $d(P_2, \mathcal{L}_1)$ is illustrated in Figures 2 as dotted green line segments. \square

2.2 Line Simplification Algorithms

Line simplification (LS) algorithms are a type of important and widely adopted trajectory compression methods, and we next briefly introduce these algorithms.

Basic Douglas-Peucker algorithm. We first introduce the Basic Douglas-Peucker (DP) algorithm [6] shown in Figure 3, the foundation of many subsequent LS algorithms.

Given a trajectory $\vec{T}[P_0, \dots, P_n]$ and an error bound ζ , algorithm DP uses the first point P_0 and the last point P_n of \vec{T} as the start point P_s and the end point P_e of the first line segment $\mathcal{L}(P_0, P_n)$, then it calculates the distance $d(P_i, \mathcal{L})$ for each point P_i ($i \in [0, n]$) (lines 1–2). If $d(P_k, \mathcal{L}) = \max\{d(P_0, \mathcal{L}), \dots, d(P_n, \mathcal{L})\} \leq \zeta$, then it returns $\{\mathcal{L}(P_0, P_n)\}$ (lines 3–5). Otherwise, it divides \vec{T} into two sub-trajectories $\vec{T}[P_0, \dots, P_k]$ and $\vec{T}[P_k, \dots, P_n]$, and recursively compresses these sub-trajectories until the entire trajectory has been considered (lines 6–7).

The DP algorithm is clearly a batch algorithm, as the entire trajectory is needed at the beginning [15], and its time complexity is $O(n^2)$. Moreover, [8] developed an improved method with a time complexity of $O(n \log n)$.

Example 2: Consider the trajectory $\vec{T}[P_0, \dots, P_{14}]$ shown in Figure 1. Algorithm DP firstly creates $\overrightarrow{P_0 P_{14}}$, then it calculates the distance of each point in $\{P_0, \dots, P_{14}\}$ to $\overrightarrow{P_0 P_{14}}$. It finds that P_{10} has the maximum distance to $\overrightarrow{P_0 P_{14}}$, which

Algorithm DP($\vec{T}[P_0, \dots, P_n], \zeta$)

1. **for** each point P_i ($i \in [0, n]$) in $\vec{T}[P_0, \dots, P_n]$ **do**
2. compute $d(P_i, \mathcal{L})$ between P_i and $\mathcal{L}(P_0, P_n)$;
3. **let** $d(P_k, \mathcal{L}) := \max\{d(P_0, \mathcal{L}), \dots, d(P_n, \mathcal{L})\}$;
4. **if** $d(P_k, \mathcal{L}) \leq \zeta$ **then**
5. **return** $\{\mathcal{L}(P_0, P_n)\}$.
6. **else**
7. **return** $\text{DP}(\vec{T}[P_0, \dots, P_k], \zeta) \cup \text{DP}(\vec{T}[P_k, \dots, P_n], \zeta)$.

Figure 3: Basic Douglas-Peucker algorithm

is greater than ζ . Then it goes to compress sub-trajectories $[P_0, \dots, P_{10}]$ and $[P_{10}, \dots, P_{14}]$, separately. Similarly, sub-trajectory $[P_0, \dots, P_{10}]$ is split to $[P_0, \dots, P_5]$ and $[P_5, \dots, P_{10}]$, and $[P_5, \dots, P_{10}]$ is split to $[P_5, \dots, P_8]$ and $[P_8, P_9, P_{10}]$. Finally, algorithm DP outputs four continuous directed line segments $\{\overrightarrow{P_0P_5}, \overrightarrow{P_5P_8}, \overrightarrow{P_8P_{10}}, \overrightarrow{P_{10}P_{14}}\}$, i.e., a piece-wise line representation of trajectory $\vec{T}[P_0, \dots, P_{14}]$ \square

Online algorithms. We next introduce two classes of DP based online algorithms that make use of sliding windows to speed up the compressing efficiency [11, 12, 15].

Given a trajectory $\vec{T}[P_0, \dots, P_n]$ and an error bound ζ , algorithm OPW [15] maintains a window $W[P_s, \dots, P_k]$, where P_s and P_k are the start and end points, respectively. Initially, $P_s = P_0$ and $P_k = P_1$, and the window W is gradually expanded by adding new points one by one. OPW tries to compress all points in $W[P_s, \dots, P_k]$ to a single line segment $\mathcal{L}(P_s, P_k)$. If the distances $d(P_i, \mathcal{L}) \leq \zeta$ for all points P_i ($i \in [s, k]$), it simply expands W to $[P_s, \dots, P_k, P_{k+1}]$ ($k+1 \leq n$) by adding a new point P_{k+1} . Otherwise, it produces a new line segment $\mathcal{L}(P_s, P_{k-1})$, and replaces W with a new window $[P_{k-1}, \dots, P_{k+1}]$. The above process repeats until all points in \vec{T} have been considered. Algorithm OPW is not efficient enough for compressing long trajectories as it remains in $O(n^2)$ time, the same as the DP algorithm.

BQS [12] reduces the compression time by introducing a convex hull that bounds a certain number of points. For a buffered sub trajectory $[P_s, \dots, P_k]$, it splits the space into four quadrants. For each quadrant, a rectangular bounding box is firstly created using the least and highest x values and the least and highest y values among points P_s, \dots, P_k . Then another two bounding lines connecting points P_s and P_h and points P_s and P_l are created such that lines $\overrightarrow{P_sP_h}$ and $\overrightarrow{P_sP_l}$ have the largest and smallest angles with the x -axis, respectively. Here $P_h, P_l \in \{P_s, \dots, P_k\}$. The bounding box and the two lines together form a convex hull. BQS picks out at most eight significant points in a quadrant. In many cases, (1) it only calculates the distances of the significant points to line $\overrightarrow{P_sP_k}$; otherwise, (2) it needs to compute all distances $d(P_i, \mathcal{L}(P_s, P_k))$ ($i \in [s, k]$) as DP. BQS remains in $O(n^2)$ time. However, its simplified version FBQS essentially avoids case (2) to achieve an $O(n)$ time complexity.

Example 3: In Figure 4, the bounding box $c_1c_2c_3c_4$ and the two lines $\overrightarrow{P_sP_h} = \overrightarrow{P_0P_1}$ and $\overrightarrow{P_sP_l} = \overrightarrow{P_0P_2}$ form a convex hull $u_1u_2c_2l_2l_1c_4$. BQS computes the distances of u_1, u_2, c_2, l_2, l_1 and c_4 to line $\overrightarrow{P_0P_6}$ when $k = 6$ or to line $\overrightarrow{P_0P_7}$ when $k = 7$.

When $k = 6$, all these distances to $\overrightarrow{P_0P_6}$ are less than ζ , hence BQS goes on to the next point (case 1); When $k = 7$, the max and min distances to $\overrightarrow{P_0P_7}$ are larger and less than ζ , respectively, and BQS needs to compress sub-trajectory $[P_0, \dots, P_7]$ along the same line as DP (case 2). \square

Error bounded algorithms. Given a trajectory \vec{T} and

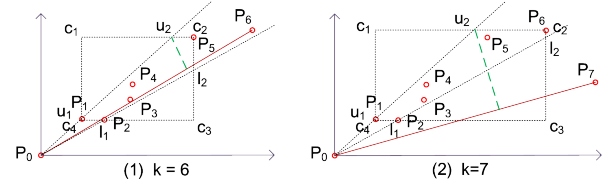


Figure 4: Examples for algorithm BQS.

its compression algorithm \mathcal{A} that produces another trajectory \vec{T}' , we say that algorithm \mathcal{A} is error bounded by ζ if for each point P in \vec{T} , there exists a point P_j in \vec{T}' with $d(P, \mathcal{L}(P_j, P_{j+1})) \leq \zeta$. Note that all the above LS algorithms are error bounded by ζ , a parameter typically set by experts based on the need and analysis of applications.

3. ONE-PASS SIMPLIFICATION

In this section, we first develop a local distance checking approach that is the key for one-pass trajectory simplification algorithms. We then present a One-Pass Error Bounded trajectory simplification algorithm, referred to as OPERB. Finally, we propose five optimization techniques.

3.1 Local Distance Checking

Existing trajectory simplification algorithms (e.g., DP [6] and online algorithms [11, 12, 15]) essentially employ a global distance checking approach to assuring error bounds, although online algorithms restrict the checking within a window. That is to say, whenever a new directed line segment $\mathcal{R}_i = \overrightarrow{P_sP_{s+i}}$ ($i \in [1, k]$) is formed for a sub-trajectory $\vec{T}_s[P_s, \dots, P_{s+k}]$, these algorithms always check its distances to all or a subset of data points $\{P_s, \dots, P_{s+i}\}$ to \mathcal{R}_i , and, therefore, a data point is checked multiple times, depending on its order in the trajectory and the number of directed line segments formed. Hence, *an appropriate local distance checking approach is needed in the first place for designing one-pass trajectory simplification algorithms.*

Consider an error bound ζ and a sub-trajectory $\vec{T}_s[P_s, \dots, P_{s+k}]$. To achieve the local distance checking, OPERB first dynamically maintains a directed line segment \mathcal{L}_i ($i \in [1, k]$), whose start point is fixed with P_s and its end point is identified (may not in $\{P_s, \dots, P_{s+i}\}$) to fit all the previously processed points $\{P_s, \dots, P_{s+i}\}$. The directed line segment \mathcal{L}_i is built by a function named *fitting function* \mathbb{F} , such that when a new point P_{s+i+1} is considered, only its distance to the directed line segment \mathcal{L}_i is checked, instead of checking the distances of all or a subset of data points of $\{P_s, \dots, P_{s+i}\}$ to $\mathcal{R}_{i+1} = \overrightarrow{P_sP_{s+i+1}}$ as the global distance checking does. In this way, a data point is checked only once during the entire process of trajectory simplification.

We next present the details of our fitting function \mathbb{F} that is designed for local distance checking.

Fitting function \mathbb{F} . Given an error bound ζ and a sub-trajectory $\vec{T}_s[P_s, \dots, P_{s+k}]$, \mathbb{F} is as follows.

$$\begin{cases} \mathcal{L}_i = \mathcal{L}_{i-1} & \text{when } (|\mathcal{R}_i| - |\mathcal{L}_{i-1}|) \leq \frac{\zeta}{4} \\ \left[\begin{array}{l} |\mathcal{L}_i| = j * \zeta/2 \\ \mathcal{L}_i.\theta = \mathcal{R}_i.\theta \end{array} \right] & \text{when } |\mathcal{R}_i| > \frac{\zeta}{4} \text{ and } |\mathcal{L}_{i-1}| = 0 \\ \left[\begin{array}{l} |\mathcal{L}_i| = j * \zeta/2 \\ \mathcal{L}_i.\theta = \mathcal{L}_{i-1}.\theta + f(\mathcal{R}_i, \mathcal{L}_{i-1}) * \arcsin\left(\frac{d(P_{s+i}, \mathcal{L}_{i-1})}{j * \zeta/2}\right) / j \end{array} \right] & \text{else} \end{cases} \quad (1) \quad (2) \quad (3)$$

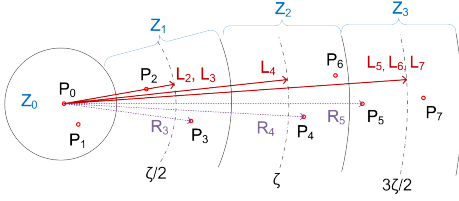


Figure 5: An example of the fitting function

where (a) $1 \leq i \leq k+1$; (b) $\mathcal{R}_{i-1} = \overrightarrow{P_s P_{s+i-1}}$, is the directed line segment whose end point P_{s+i-1} is in $\ddot{\mathcal{T}}_s[P_s, \dots, P_{s+k}]$; (c) \mathcal{L}_i is the directed line segment built by fitting function \mathbb{F} to fit sub-trajectory $\ddot{\mathcal{T}}_s[P_s, \dots, P_{s+i}]$ and $\mathcal{L}_0 = \mathcal{R}_0$; (d) $j = \lceil (|\mathcal{R}_i| * 2/\zeta - 0.5) \rceil$; (e) $f(\cdot)$ is a sign function such that $f(\mathcal{R}_i, \mathcal{L}_{i-1}) = 1$ if the included angle $\angle(\mathcal{R}_{i-1}, \mathcal{R}_i) = (\mathcal{R}_i.\theta - \mathcal{L}_{i-1}.\theta)$ falls in the range of $(-2\pi, -\frac{3\pi}{2}]$, $[-\pi, -\frac{\pi}{2}]$, $[0, \frac{\pi}{2}]$ and $[\pi, \frac{3\pi}{2})$, and $f(\mathcal{R}_i, \mathcal{L}_{i-1}) = -1$, otherwise; (f) $\zeta/2$ is a step length to control the increment of $|\mathcal{L}|$.

Given any sub-trajectory $\ddot{\mathcal{T}}_s[P_s, \dots, P_{s+k}]$ and any error bound ζ , the expression $j = \lceil (|\mathcal{R}_i| * 2/\zeta - 0.5) \rceil$ in the fitting function \mathbb{F} essentially partitions the space into zones around the center point P_s such that for each $j \geq 0$, zone $Z_j = \{P_j \mid j * \zeta/2 - \zeta/4 < |\overrightarrow{P_s P_j}| \leq j * \zeta/2 + \zeta/4\}$, i.e., the radii of Z_0, Z_1, Z_2 and Z_3 to P_s are in the ranges of $(-\frac{1}{4}\zeta, \frac{1}{4}\zeta]$, $(\frac{1}{4}\zeta, \frac{3}{4}\zeta]$, $(\frac{3}{4}\zeta, \frac{5}{4}\zeta]$ and $(\frac{5}{4}\zeta, \frac{7}{4}\zeta]$, respectively, and all ranges have a fixed size $\zeta/2$ as shown in Figure 5. Moreover, the angle of the directed line segment \mathcal{L}_i is adjusted from \mathcal{L}_{i-1} to make it closer to P_{s+i} than \mathcal{L}_{i-1} , i.e., $d(P_{s+i}, \mathcal{L}_i) \leq d(P_{s+i}, \mathcal{L}_{i-1})$ for any $i \in (s, s+k]$, and the angle from \mathcal{L}_1 to \mathcal{L}_k is bounded by a constant (Lemma 3).

The fitting function \mathbb{F} also creates a virtual stepwise sub-trajectory $\ddot{\mathcal{T}}_v[V_s, \dots, V_{s+l}]$ such that $V_s = P_s$, $|\overrightarrow{V_s V_{s+j}}| = \zeta/2 * j$ ($j \in [0, l], 0 < l \leq k$). For each point P_{s+i} in the sub-trajectory, it is mapped to a virtual point V_{s+j} in $\ddot{\mathcal{T}}_v$ locating in zone Z_j . Observe that (a) it is possible that $(|\mathcal{R}_i| - |\mathcal{L}_{i-1}|) \leq 0$, (b) the fitting function \mathbb{F} forms a directed line segment \mathcal{L}_i , which is closer to \mathcal{R}_i than \mathcal{L}_{i-1} , and partitions the points in the sub-trajectory $\ddot{\mathcal{T}}$ into two classes:

(1) *Active points.* Points P_s and P_{s+i} such that $|\mathcal{R}_i| - |\mathcal{L}_{i-1}| > \zeta/4$ are referred to as active points. An active point P_{s+i} is mapped to the virtual point in zone Z_j with $j = \lceil (|\mathcal{R}_i| * 2/\zeta - 0.5) \rceil$, and each zone has at most one active point.

(2) *Inactive points.* Points P_{s+i} such that $|\mathcal{R}_i| - |\mathcal{L}_{i-1}| \leq \zeta/4$ are referred to as inactivated points. For an inactive point P_{s+i} , it is mapped to zone Z_j with $j = \lfloor |\mathcal{L}_{i-1}| * 2/\zeta \rfloor$. There may exist none or multiple inactive points in a zone.

We next explain the fitting function \mathbb{F} with an example.

Example 4: Consider the sub-trajectory $[P_0, \dots, P_7]$ in Figure 5 whose eight points fall in zones Z_0, Z_1, Z_2, Z_3 .

(1) Point P_0 is the start point and the first active point, and $\mathcal{L}_0 = \mathcal{R}_0 = \overrightarrow{P_0 P_0}$.

(2) Point P_1 is inactive in zone Z_0 , as $|\mathcal{R}_1| = |\overrightarrow{P_0 P_1}| < \frac{\zeta}{4}$ and $(|\mathcal{R}_1| - |\mathcal{L}_0|) \leq \frac{\zeta}{4}$. Hence, $\mathcal{L}_1 = \mathcal{L}_0$ (case (1)).

(3) Point P_2 is active in Z_1 , as $|\mathcal{R}_2| > \frac{\zeta}{4}$ and $|\mathcal{L}_1| = 0$. Hence, $|\mathcal{L}_2| = \frac{\zeta}{2}$ and $\mathcal{L}_2.\theta = \mathcal{R}_2.\theta$ (case (2)).

(4) Point P_3 is inactive in Z_1 , as $(|\mathcal{R}_3| - |\mathcal{L}_2|) \leq \frac{\zeta}{4}$. Hence, $\mathcal{L}_3 = \mathcal{L}_2$ (case (1)).

(5) Point P_4 is active in Z_2 , as $|\mathcal{R}_4| - |\mathcal{L}_3| > \frac{\zeta}{4}$ and $|\mathcal{L}_3| \neq 0$. Hence, $|\mathcal{L}_4| = 2 * \frac{\zeta}{2} = \zeta$ and the angle of \mathcal{L}_4 is also calculated

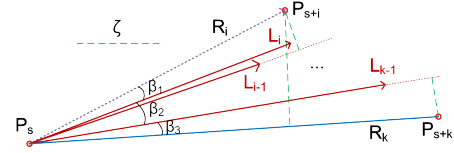


Figure 6: Example for the proof of Lemma 4

accordingly (case 3).

(6) Similarly, point P_5 is active in Z_3 (case 3), and points P_6 and P_7 are inactive (case 1). Here P_6 is mapped to Z_3 as $|\mathcal{L}_5| = \frac{3}{2}\zeta$ though it is physically located in zone Z_2 . \square

3.2 Analyses of the Fitting Function

We next give an analysis of the fitting function \mathbb{F} . First, by the definition of \mathbb{F} , it is easy to have the following.

Proposition 1: Given any sub-trajectory $\ddot{\mathcal{T}}_s[P_s, \dots, P_{s+k}]$ and error bound ζ , the directed line segment \mathcal{L}_i ($i \in [1, k]$) can be computed by the fitting function \mathbb{F} in $O(1)$ time. \square

The fitting function \mathbb{F} also enables a local distance checking method, as shown below.

Theorem 2: Given any sub-trajectory $\ddot{\mathcal{T}}_s[P_s, \dots, P_{s+k}]$ with $k \leq 4 \times 10^5$ and error bound ζ , then $d(P_{s+i}, \overrightarrow{P_s P_{s+k}}) \leq \zeta$ for each $i \in [0, k]$ if P_{s+k} is an active point and $d(P_{s+i}, \mathcal{L}_{i-1}) \leq \zeta/2$ for each $i \in [1, k]$. \square

To prove Theorem 2, we first introduce a special class of trajectories, based on which we show that Theorem 2 holds.

Stepwise trajectories. We say that a trajectory $\ddot{\mathcal{T}}[P_s, \dots, P_{s+k}]$ is stepwise w.r.t. $\zeta/2$ if and only if $|\mathcal{R}_i| = i * \zeta/2$ for each directed line segment $\mathcal{R}_i = \overrightarrow{P_s P_{s+i}}$ ($i \in [0, k]$).

Observe that $|\mathcal{R}_i| - |\mathcal{R}_{i-1}| = \zeta/2$ and $\lceil |\mathcal{R}_i| * 2/\zeta - 0.5 \rceil = i$ ($i \in [1, k]$). Hence, for stepwise sub-trajectories $\ddot{\mathcal{T}}[P_s, \dots, P_{s+k}]$, the fitting function can be simplified as \mathbb{F}' below.

$$\begin{cases} \begin{cases} |\mathcal{L}_1| = \zeta/2 \\ |\mathcal{L}_1.\theta = \mathcal{R}_1.\theta \end{cases} & i = 1 \quad (1) \\ \begin{cases} |\mathcal{L}_i| = i * \zeta/2 \\ \mathcal{L}_i.\theta = \mathcal{L}_{i-1}.\theta + f(\mathcal{R}_i, \mathcal{L}_{i-1}) * \arcsin(\frac{d(P_{s+i}, \mathcal{L}_{i-1})}{i * \zeta/2})/i \end{cases} & i \geq 2 \quad (2) \end{cases}$$

Stepwise trajectories have the following properties.

Lemma 3: Given any sub-trajectory $\ddot{\mathcal{T}}_s[P_s, \dots, P_{s+k}]$ and error bound ζ , if $d(P_{s+i}, \mathcal{L}_{i-1}) \leq \frac{\zeta}{2}$ for each $i \in [2, k]$, then the angle change between \mathcal{L}_1 and \mathcal{L}_k is bounded by $\Delta\theta = \lim_{k \rightarrow \infty} \sum_{i=2}^k \frac{1}{i} * \arcsin(\frac{1}{i}) < 0.8123$ (or 46.54°). \square

Proof: By the revised fitting function \mathbb{F}' for a stepwise sub-trajectory and $d(P_{s+i}, \mathcal{L}_{i-1}) \leq \frac{\zeta}{2}$ for all $i \in [2, k]$, we have $\Delta\theta \leq \sum_{i=2}^k \frac{1}{i} * \arcsin(\frac{1}{i})$, which is monotonically increasing with the increment of k . As $x \leq \arcsin(x) \leq x/\sqrt{1-x^2}$ ($0 \leq x < 1$), we also have $\frac{1}{i} \leq \arcsin \frac{1}{i} \leq 1/\sqrt{i^2-1}$ ($i \geq 2$).

Hence, we have $\Delta\theta \leq \lim_{k \rightarrow \infty} \sum_{i=2}^k (\frac{1}{i} * \frac{1}{\sqrt{i^2-1}}) < \int_2^\infty (\frac{1}{x} * \frac{1}{\sqrt{x^2-1}}) dx + \frac{1}{2} * \frac{1}{\sqrt{2^2-1}} = \frac{\pi}{6} + \frac{1}{2\sqrt{3}} \approx 0.8123$. \square

Lemma 4: Given any sub-trajectory $\ddot{\mathcal{T}}_s[P_s, \dots, P_{s+k}]$ with $k \leq 4 \times 10^5$ and error bound ζ , then $d(P_{s+i}, \overrightarrow{P_s P_{s+k}}) \leq \zeta$ for each $i \in [0, k]$ if $d(P_{s+i}, \mathcal{L}_{i-1}) \leq \frac{\zeta}{2}$ for each $i \in [1, k]$. \square

Algorithm OPERB($\ddot{T}[P_0, \dots, P_n], \zeta$)

```

1.  $\bar{T} := \emptyset$ ;  $P_e := P_0$ ;  $(P_a, flag) := \text{getActivePoint}(\ddot{T}, P_0, P_0, \mathcal{L}_0, \zeta)$ ;
2. while  $P_a \neq \text{nil}$  do {
3.    $P_s := P_e$ ;  $\mathcal{L}_a := \mathbb{F}(P_a, \overrightarrow{P_s P_s})$ ;
4.    $(P_a, flag) := \text{getActivePoint}(\ddot{T}, P_s, P_a, \mathcal{L}_a, \zeta)$ ;
5.   while  $P_a \neq \text{nil}$  &  $flag = \text{true}$  do {
6.      $\mathcal{L}_a := \mathbb{F}(P_a, \mathcal{L}_a)$ ;  $P_e := P_a$ ;
7.      $(P_a, flag) := \text{getActivePoint}(\ddot{T}, P_s, P_a, \mathcal{L}_a, \zeta)$ ; }
8.    $\bar{T} := \bar{T} \cup \{P_s P_e\}$ ; }
9. return  $\bar{T}$ .

```

Procedure $\text{getActivePoint}(\ddot{T}, P_s, P_a, \mathcal{L}_a, \zeta)$

```

1.  $i := a + 1$ ;  $flag := \text{true}$ ;
2. while  $(|\mathcal{R}_i| - |\mathcal{L}_a|) \leq \zeta/4$  &  $i \leq n$  &  $(i - s) \leq 4 \times 10^5$  do {
3.   if  $d(P_i, \mathcal{L}_a) > \zeta/2$  or  $d(P_i, \mathcal{R}_a) > \zeta$  then
4.      $flag := \text{false}$ ; break;
5.    $i := i + 1$ ; }
6. if  $d(P_i, \mathcal{L}_a) > \zeta/2$  &  $|\mathcal{L}_a| > 0$  then  $flag := \text{false}$ ;
7. if  $i = n + 1$  then  $P_i := \text{nil}$ ;
8. return  $(P_i, flag)$ .

```

Figure 7: Algorithm OPERB

Proof: Consider the four directed line segments $\mathcal{R}_i = \overrightarrow{P_s P_{s+i}}$, $\mathcal{R}_k = \overrightarrow{P_s P_{s+k}}$, \mathcal{L}_{i-1} and \mathcal{L}_{k-1} shown in Figure 6. Further, let $\beta_1 = \mathcal{R}_i \cdot \theta - \mathcal{L}_{i-1} \cdot \theta$, $\beta_2 = \mathcal{L}_{k-1} \cdot \theta - \mathcal{L}_i \cdot \theta$, $\beta_3 = \mathcal{R}_k \cdot \theta - \mathcal{L}_{k-1} \cdot \theta$. We then adjust the included angles β_1 as follows: (a) if $\frac{\pi}{2} < |\beta_1| \leq \pi$, $\beta_1 = \pi - \beta_1$, (b) if $\pi < |\beta_1| \leq \frac{3}{2}\pi$, $\beta_1 = \beta_1 - \pi$, (c) if $\frac{3}{2}\pi < |\beta_1| \leq 2\pi$, $\beta_1 = 2\pi - \beta_1$, and (d) $\beta_1 = |\beta_1|$, otherwise. The included angle β_3 is adjusted along the same line as β_1 , and β_2 is bounded by Lemma 3.

Observe that $d(P_{s+i}, \mathcal{R}_k) \leq i * \frac{\zeta}{2} * \sin(|\beta_1| + |\beta_2| + |\beta_3|) \leq i * \frac{\zeta}{2} * \sin(\arcsin \frac{1}{i} + \sum_{j=i+1}^{k-1} (\frac{1}{j} * \arcsin \frac{1}{j}) + \arcsin \frac{1}{k})$. For any $k \leq 4 \times 10^5$, $i * \sin(|\beta_1| + |\beta_2| + |\beta_3|) < 2$, and, hence, we have $d(P_{s+i}, \mathcal{R}_k) < \frac{\zeta}{2} * 2 = \zeta$. \square

By mapping inactive and active points of a trajectory to virtual points of a trajectory stepwise *w.r.t.* $\zeta/2$, one can readily prove Theorem 2 along the lines as Lemma 4.

Remarks. (1) Our fitting function achieves local distance checking, as indicated by Proposition 1 and Theorem 2; (2) For a sub-trajectory $\ddot{T}_s[P_s, \dots, P_{s+k-1}]$ represented by a single directed line segment, we restrict $k \leq 4 \times 10^5$, which suffices for the need of trajectory simplification in practice.

3.3 Algorithm OPERB

We are now ready to present our one-pass error bounded algorithm, which makes use of the local distance checking method based on the fitting function \mathbb{F} .

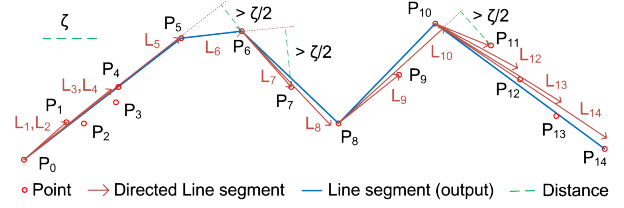
The main result of this section is as follows.

Theorem 5: *Given any trajectory $\ddot{T}[P_0, \dots, P_n]$ and error bound ζ , there exists a one-pass trajectory simplification algorithm that is error bounded by ζ .* \square

We prove Theorem 5 by providing such an algorithm for trajectory simplification, referred to as OPERB shown in Figure 7. Given a trajectory $\ddot{T}[P_0, \dots, P_n]$ and an error bound ζ as input, algorithm OPERB outputs a compression trajectory, *i.e.*, a piecewise line representation \bar{T} of \ddot{T} .

We first describe its procedure, and then present OPERB.

Procedure getActivePoint . It takes as input a trajectory \ddot{T} , a start point P_s , the current active point P_a , the current directed line segment \mathcal{L}_a and the error bound ζ , and finds the next active point P_i . (1) When $P_i = \text{nil}$, it means that no more active points could be found in the remaining sub-


Figure 8: A running example of algorithm OPERB.

trajectory $\ddot{T}[P_s, \dots, P_n]$; (2) When $flag = \text{true}$, it means that the next active point P_i can be combined with the current directed line segment \mathcal{L}_a to form a new directed line segment; Otherwise, (3) a new line segment should be generated, and a new start point is considered.

It first increases a by 1 as it considers the data points after P_a , and sets $flag$ to *true* (line 1). Secondly, by the definition of the fitting function \mathbb{F} , it finds the next active point P_i (lines 2–6). Thirdly, if $i = n + 1$, then all data points in \ddot{T} have been considered, hence, P_i is set to *nil* (line 7). Finally, $(P_i, flag)$ is returned (line 8).

Algorithm OPERB. It takes as input a trajectory \ddot{T} and an error bound ζ , and returns the simplified trajectory \bar{T} .

After initializing (line 1), it then repeatedly processes the data points in \ddot{T} one by one until all data points have been considered, *i.e.*, $P_a = \text{nil}$ (lines 2–8). If P_a is not *nil* and $flag$ is *true*, it means that P_a can be combined with the current directed line segment \mathcal{L}_a (lines 5–7). If $flag$ is *false*, then a directed line segment $\overrightarrow{P_s P_e}$ is generated and added to \bar{T} (line 8). Finally, the set \bar{T} of directed line segments, *i.e.*, a piecewise line segmentation of \ddot{T} , is returned (line 9).

We next explain algorithm OPERB with an example.

Example 5: Algorithm OPERB takes as input the trajectory and ζ shown in Figure 1, and its output is illustrated in Figure 8. The process of algorithm OPERB is as follows.

- (1) It initializes \bar{T} with \emptyset , the last active point P_e with P_0 and the current active point P_a with P_1 (line 1).
- (2) As $P_a \neq \text{nil}$ (line 2), it then sets $P_s = P_e = P_0$ and $\mathcal{L}_a = \mathbb{F}(P_a, \overrightarrow{P_s P_s}) = \mathbb{F}(P_1, \overrightarrow{P_0 P_0}) = \mathcal{L}_1$ (line 3).
- (3) It then calls $\text{getActivePoint}()$ to get the next active point $P_a = P_3$ and $flag = \text{true}$ (line 4). As $flag = \text{true}$ means that P_3 can be combined with the current line segment $\mathcal{L}_a = \mathcal{L}_1$, so it updates \mathcal{L}_a to \mathcal{L}_3 , and P_e to P_3 (line 6).
- (4) Then it continues reading the next active point $P_a = P_5$ with $flag = \text{true}$ (line 7), and updates the current line segment \mathcal{L}_a to \mathcal{L}_5 , and P_e to P_5 (lines 5, 6).
- (5) It gets the next active $P_a = P_6$ and $flag = \text{false}$, as $d(P_6, \mathcal{L}_5) > \frac{\zeta}{2}$, meaning that P_6 should not be compressed to the current directed line segment (line 5). Hence, it adds $\overrightarrow{P_s P_e} = \overrightarrow{P_0 P_5}$ to \bar{T} (line 8), sets $P_s = P_e = P_5$, and updates \mathcal{L}_a to $\mathbb{F}(P_a, \overrightarrow{P_s P_s}) = \mathbb{F}(P_6, \overrightarrow{P_5 P_5}) = \mathcal{L}_6$ (line 3).
- (6) The process continues until all points have been processed. At last, the algorithm outputs five continuous line segments $\{\overrightarrow{P_0 P_5}, \overrightarrow{P_5 P_6}, \overrightarrow{P_6 P_8}, \overrightarrow{P_8 P_{10}}, \overrightarrow{P_{10} P_{14}}\}$. \square

Correctness & complexity analysis. The correctness of algorithm OPERB follows from Theorem 2 immediately. Observe that for a trajectory \ddot{T} with n data points, the fitting function \mathbb{F} is called at most n times, and each data point is considered once and only once. By Proposition 1, algorithm OPERB runs in $O(n)$ time. It is also easy to verify that algorithm OPERB takes $O(1)$ space, as the directed line segment

in $\bar{\mathcal{T}}$ can be output immediately once it is generated.

Note that this also completes the proof of Theorem 5.

3.4 Optimization Techniques

We further propose five optimization techniques for OPERB to achieve a better compression ratio. The key idea behind this is to (1) compress as many points as possible with a directed line segment, or (2) to let the directed line segment \mathcal{L}_i as close as possible to the current active point P_i so that it has a higher possibility to represent P_{i+1} . These optimization techniques are organized by the processing order from the start to the end points of directed line segments.

(1) Choosing the first active point after P_s . Algorithm OPERB calls procedure `getActivePoint` to get the first active point P_a in a sub-trajectory $\bar{\mathcal{T}}[P_{s+1}, \dots, P_{s+k}]$ such that $|\overrightarrow{P_s P_a}| > \zeta/4$ (line 4 in Figure 7). However, as indicated by the fitting function \mathbb{F} , we can replace P_a with the first point P_b such that $|\overrightarrow{P_s P_b}| > \zeta$, without affecting the boundness of algorithm OPERB. This method potentially improves the compression ratio because more points are covered by the directed line segment $\overrightarrow{P_s P_b}$ than $\overrightarrow{P_s P_a}$, and $\overrightarrow{P_s P_b}$ is also closer to P_b than $\overrightarrow{P_s P_a}$.

(2) Adjusting the distance condition. Given any sub-trajectory $\bar{\mathcal{T}}[P_s, \dots, P_{s+k}]$ and error bound ζ , let $d_{max}^+ = \max\{d(P_{s+i}, \mathcal{L}_{i-1}) \mid f(\mathcal{R}_i, \mathcal{L}_{i-1}) = 1 \text{ and } i \in [1, k]\}$ and $d_{max}^- = \max\{d(P_{s+i}, \mathcal{L}_{i-1}) \mid f(\mathcal{R}_i, \mathcal{L}_{i-1}) = -1 \text{ and } i \in [s+1, s+k]\}$. Then the condition $d(P_{s+i}, \mathcal{L}_{i-1}) \leq \zeta/2$ in Theorem 2 can be replaced with $d_{max}^- + d_{max}^+ \leq \zeta$, and algorithm OPERB remains error bounded by ζ . Say, if $d_{max}^+ = 0.3\zeta$ and $d_{max}^- = 0.6\zeta$, then $d(P_{s+i}, \mathcal{L}_k)$ for each $i \in [s, s+k]$ is still less than $0.3\zeta + 0.6\zeta = 0.9\zeta < \zeta$.

Note that $d(P_{s+i}, \mathcal{L}_{i-1}) \leq \zeta/2$ implies $d_{max}^+ \leq \zeta/2$ and $d_{max}^- \leq \zeta/2$, and, hence, $d_{max}^- + d_{max}^+ \leq \zeta$. Therefore, $d(P_{s+i}, \mathcal{L}_{i-1}) \leq \zeta/2$ is a special case of $d_{max}^- + d_{max}^+ \leq \zeta$.

(3) Making \mathcal{L} more close to the active points. When OPERB calculates the angle $\mathcal{L}_i.\theta$ of an active point P_i , the factor $d(P_i, \mathcal{L}_{i-1})$ in the fitting function \mathbb{F} can be replaced by a bigger number d_x such that $0 \leq d_x \leq d_{max}^-$ when $f(\mathcal{R}_i, \mathcal{L}_{i-1}) = -1$ or $0 \leq d_x \leq d_{max}^+$ when $f(\mathcal{R}_i, \mathcal{L}_{i-1}) = 1$, to let \mathcal{L}_i be more close to P_i , under the restriction that $(\arcsin(\frac{d_x}{j*\zeta/2})/j)$ is not larger than $\arcsin(\frac{d(P_i, \mathcal{L}_{i-1})}{j*\zeta/2})$.

(4) Incorporating missing active points. For a sub-trajectory $\bar{\mathcal{T}}[P_s, \dots, P_a, \dots, P_{a+i}, \dots, P_{s+k}]$, whereas P_a and P_{a+i} are two consecutive active points. Let $j_a = \lceil (|\mathcal{R}_a| * 2/\zeta - 0.5) \rceil$, $j_{a+1} = \lceil (|\mathcal{R}_{a+i}| * 2/\zeta - 0.5) \rceil$ and $\Delta j = j_{a+1} - j_a$. If $\Delta j > 1$, then there are no active points between zones Z_{j_a} and $Z_{j_{a+1}}$. In this case, we replace $\mathcal{L}_{a+i}.\theta$ with $\mathcal{L}_{a+i-1}.\theta + f(\mathcal{R}_{a+i}, \mathcal{L}_{a+i-1}) * \arcsin(\frac{d(P_{a+i}, \mathcal{L}_{a+i-1})}{j_{a+1}*\zeta/2}) * \frac{\Delta j}{j_{a+1}}$ for the fitting function \mathbb{F} , instead of $\mathcal{L}_{a+i-1}.\theta + f(\mathcal{R}_{a+i}, \mathcal{L}_{a+i-1}) * \arcsin(\frac{d(P_{a+i}, \mathcal{L}_{a+i-1})}{j_{a+1}*\zeta/2}) * \frac{1}{j_{a+1}}$ to compensate the side effects of missing active points to make the line \mathcal{L}_{a+i} more closer to P_{a+i} . Note that $\mathcal{L}_{a+i-1} = \mathcal{L}_a$ and $\Delta j > 0$. Moreover, $d(P_{a+i}, \mathcal{L}_{a+i-1})$ could also be replaced by d_x as above.

(5) Absorbing data points after P_{s+k} . Given any sub-trajectory $\bar{\mathcal{T}}_s[P_s, \dots, P_{s+k}, \dots, P_{s+t}]$ and error bound ζ , if $[P_s, \dots, P_{s+k}]$ is compressed to a line segment $\overrightarrow{P_s P_{s+k}}$, then any point P_{s+t} ($t > k$) can also be compressed to $\overrightarrow{P_s P_{s+k}}$ as long as $d(P_{s+t}, \overrightarrow{P_s P_{s+k}}) \leq \zeta$ such that OPERB can compress more points into the directed line segment.

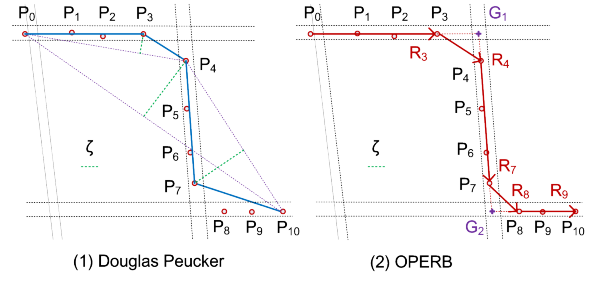


Figure 9: Example anomalous line segments: the compression results of algorithms DP and OPERB on a sub-trajectory with eleven points collected from a moving vehicle running on an urban road network.

Remark. These optimization techniques are seamlessly integrated into OPERB, and Theorem 5 remains intact.

4. AN AGGRESSIVE APPROACH

In this section, we introduce an aggressive one-pass trajectory simplification algorithm, referred to as OPERB-A, which extends algorithm OPERB by further allowing trajectory interpolation under certain conditions, and even achieves a better compression ratio than algorithm DP, the existing LS algorithm with the best compression ratio.

4.1 Trajectory Interpolation

Existing line simplification algorithms, even the global distance checking algorithm DP and our algorithm OPERB, may generate a set of *anomalous line segments*.

Anomalous line segments. Consider a trajectory $\bar{\mathcal{T}}[P_0, \dots, P_n]$ and its piece-wise line representation $\bar{\mathcal{T}}[\mathcal{R}_0, \dots, \mathcal{R}_m]$ ($0 < m \leq n$) generated by an LS algorithm. A line segment \mathcal{R}_i ($i \in [0, m]$) is anomalous if it only represents two data points in $\bar{\mathcal{T}}$, i.e., its own start and end points.

Anomalous line segments impair the effectiveness of trajectory simplification. We illustrate this with an example.

Example 6: Let us consider the compressing results of algorithms DP and OPERB on a sub-trajectory, shown in Figure 9, which has one crossroad between data points P_3 and P_4 , and another crossroad between data points P_7 and P_8 . Given the sub-trajectory and the error bound as shown in Figure 9, algorithm DP returns four directed line segments $\{\overrightarrow{P_0 P_3}, \overrightarrow{P_3 P_4}, \overrightarrow{P_4 P_7}, \overrightarrow{P_7 P_{10}}\}$, and algorithm OPERB outputs five directed line segments $\{\overrightarrow{P_0 P_3}, \overrightarrow{P_3 P_4}, \overrightarrow{P_4 P_7}, \overrightarrow{P_7 P_8}, \overrightarrow{P_8 P_{10}}\}$, respectively. Observe that the directed line segments $\overrightarrow{P_3 P_4}$ and $\overrightarrow{P_7 P_8}$ are anomalous. \square

In this work, we propose the use of interpolating new data points, referred to as *patch points*, into a trajectory under certain conditions to reduce the number of anomalous line segments to a large extent. The rational behind this is that moving objects have sudden track changes while certain important data points may not be sampled due to various reasons, especially on urban road networks. Note that slightly changing the lines has proven useful in other disciplines [17].

Patch points. Let \mathcal{R}_{i-1} , \mathcal{R}_i and \mathcal{R}_{i+1} be three continuous directed line segments, where \mathcal{R}_i is anomalous, i.e., \mathcal{R}_i represents only two points. The patch point G w.r.t. \mathcal{R}_i is the intersection point between line segments \mathcal{R}_{i-1} and \mathcal{R}_{i+1} .

We next illustrate the use of patch points for reducing anomalous line segments with an example.

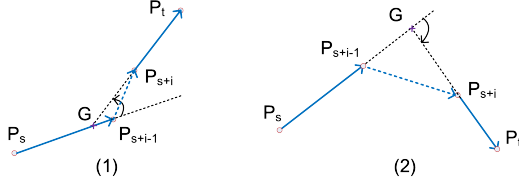


Figure 10: Practical restrictions on patch points.

Example 7: Consider Figure 9(2), where G_1, G_2 are the patch points *w.r.t.* \mathcal{R}_4 and \mathcal{R}_8 , respectively. After G_1 and G_2 are interpolated, both algorithms DP and OPERB return three directed line segments $\{\overrightarrow{P_0G_1}, \overrightarrow{G_1G_2}, \overrightarrow{G_2P_{10}}\}$, instead of four and five, respectively, as shown in Example 6. \square

Patching method. Consider any three continuous directed line segments, $\mathcal{R}_{i-1} = \overrightarrow{P_s P_{s+i-1}}$, $\mathcal{R}_i = \overrightarrow{P_{s+i-1} P_{s+i}}$ and $\mathcal{R}_{i+1} = \overrightarrow{P_{s+i} P_t}$ such that \mathcal{R}_i is anomalous and point P_t is an active point and $t > s+i$. With the practical restrictions and one-pass requirement, the patch point G *w.r.t.* \mathcal{R}_i needs to satisfy the conditions below, as illustrated by Figure 10.

- (1) Lying on the lines of $\overrightarrow{P_s P_{s+i-1}}$ (i.e., $\overrightarrow{P_s G} \cdot \theta = \overrightarrow{P_s P_{s+i-1}} \cdot \theta$) and $\overrightarrow{P_{s+i} P_t}$ (i.e., $\overrightarrow{G P_{s+i}} \cdot \theta = \overrightarrow{P_{s+i} P_t} \cdot \theta$),
- (2) $|\overrightarrow{P_s G}| \geq (|\overrightarrow{P_s P_{s+i-1}}| - \zeta/2)$, and
- (3) the included angle from \mathcal{R}_{i-1} to \mathcal{R}_{i+1} falls in $(-2\pi, -\pi - \gamma_m]$, $[\gamma_m - \pi, \pi - \gamma_m]$ and $[\pi + \gamma_m, 2\pi)$, where $\gamma_m \in [0, \pi]$ is a parameter with $\gamma_m = \frac{\pi}{3}$ by default.

Intuitively, these conditions are to incorporate the sudden changes of moving directions implied in a trajectory. Note that the restriction of the included angles may reduce the chance of eliminating anomalous line segments. However, it helps to produce more rational results.

4.2 Algorithm OPERB-A

We now present our algorithm OPERB-A that extends algorithm OPERB by introducing patch points. Recall that algorithm OPERB starts a new directed line segment when the distance of a point, say P_i , to the line segment \mathcal{L}_{i-1} is larger than $\zeta/2$, marks the last active point P_a as P_{s+i-1} , outputs the directed line segment $\mathcal{R}_{i-1} = \overrightarrow{P_s P_{s+i-1}}$, and marks P_{s+i-1} as the new start point P_s of the remaining subjectify $\mathcal{T}_s[P_{s+i-1}, \dots, P_n]$. However, for OPERB-A, the line segment \mathcal{R}_{i-1} cannot be outputted until the patch point G is determined when $\mathcal{R}_i = \overrightarrow{P_{s+i-1} P_{s+i}}$ is an AL, and patch point G cannot be determined unless the angle of $\mathcal{R}_{i+1} = \overrightarrow{P_{s+i} P_t}$ has been determined. Hence, different from OPERB, OPERB-A uses a lazy output policy.

The lazy output policy. OPERB-A temporarily saves a line segment in memory before outputting it, as follows:

- (1) For simplicity, suppose that the line segment \mathcal{R}_{i-1} is not anomalous and cannot be compressed with any more points. OPERB-A saves it in memory first.
- (2) It then compresses the subsequent points as OPERB to the next line segment \mathcal{R}_i until a broken condition is triggered. If \mathcal{R}_i is not anomalous, then it outputs \mathcal{R}_{i-1} and saves \mathcal{R}_i in memory. Otherwise, it marks \mathcal{R}_i anomalous, saves it, and moves to the next line segment \mathcal{R}_{i+1} .
- (3) If \mathcal{R}_{i+1} is determined and \mathcal{R}_i is anomalous, OPERB-A checks the possibility of patching a point G *w.r.t.* \mathcal{R}_i . If so, it outputs $\overrightarrow{P_s G}$, and $\overrightarrow{G P_{s+i}}$ is temporarily saved; Otherwise, it outputs \mathcal{R}_{i-1} and \mathcal{R}_i , and \mathcal{R}_{i+1} is temporarily saved.
- (4) The process repeats until all points have been processed.

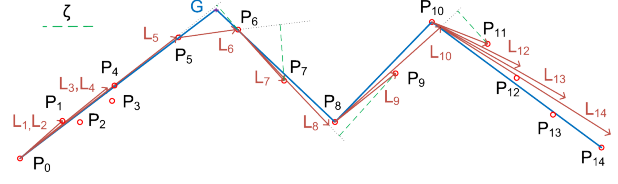


Figure 11: A running example of OPERB-A.

Remarks. All the optimization techniques in Section 3.4 remain intact, and are seamlessly integrated into OPERB-A.

We next explain algorithm OPERB-A with an example.

Example 8: Algorithm OPERB-A takes as input the trajectory and ζ shown in Figure 1, and its output is illustrated in Figure 11. The process of OPERB-A is as follows.

- (1) It first creates $\mathcal{L}_0 = \mathcal{R}_0 = \overrightarrow{P_0 P_0}$, compresses P_1, \dots, P_5 in turn, and generates \mathcal{L}_5 , along the same lines as OPERB.
- (2) It then finds that $d(P_6, \mathcal{L}_5) > \zeta/2$, which means that P_6 cannot be compressed into $\mathcal{R}_5 = \overrightarrow{P_0 P_5}$. \mathcal{R}_5 is temporally saved. And the next line segment starts from P_5 .
- (3) It then finds that $d(P_7, \mathcal{L}_6) > \zeta/2$ and $\mathcal{R}_6 = \overrightarrow{P_5 P_6}$ is an AL. Hence, \mathcal{R}_6 is also temporally saved, and the next line segment starts from P_6 .
- (4) It continues to compress points P_7 and P_8 in turn, and generates \mathcal{L}_8 along the same lines as OPERB.
- (5) It then finds that $d(P_9, \mathcal{L}_8) > \zeta/2$, which means that $\mathcal{R}_8 = \overrightarrow{P_6 P_8}$ is determined. Now OPERB-A tries to expand the lines of \mathcal{R}_5 and \mathcal{R}_8 to get the intersection point G of them, and uses it as the final start point of \mathcal{R}_8 . At last, \mathcal{R}_5 is extended to $\overrightarrow{P_0 G}$ and output as a directed line segment in the result, $\overrightarrow{G P_8}$ is temporarily saved and P_8 becomes the start point of the next line segment.
- (6) The above process repeats until all points have been processed. Finally, OPERB-A outputs four line segments $\{\overrightarrow{P_0 G}, \overrightarrow{G P_8}, \overrightarrow{P_8 P_{10}}, \overrightarrow{P_{10} P_{14}}\}$.

As shown in Figure 11, algorithm OPERB-A further eliminates the directed line segment $\overrightarrow{P_5 P_6}$, compared with the result of OPERB shown in Figure 8. \square

Correctness & complexity analysis. Observe that algorithm OPERB-A does not change the angle of any directed line segment compared with OPERB, and hence it remains error bounded. Moreover, each data point in a trajectory is read once and only once in OPERB-A. Therefore, algorithm OPERB-A is one-pass and error bounded. It is also easy to verify that algorithm OPERB-A takes $O(1)$ space, the same as OPERB, as the directed line segment in \mathcal{T} can be outputted immediately once it is generated. That is, the nice properties of OPERB remain intact in OPERB-A.

5. EXPERIMENTAL STUDY

In this section, we present an extensive experimental study of our one-pass error bounded algorithms OPERB and OPERB-A. Using four real-life datasets, we conducted four sets of experiments to evaluate: (1) the execution time of our approaches compared with algorithms DP and FBQS, and the impacts of optimizations, (2) the compression ratios of our approaches compared with DP and FBQS, and the impacts of optimizations, (3) the average errors of our approaches compared with algorithms DP and FBQS, and (4) the effectiveness of trajectory interpolation.

Data Sets	Number of Trajectories	Sampling Rates(s)	PointsPer Trajectory(K)	Total points
Taxi	12,727	60	~ 39.1	498M
Truck	10,368	1-60	~ 71.9	746M
SerCar	11,000	3-5	~ 119.1	1.31G
GeoLife	182	1-5	~ 132.8	24.2M

Table 1: Real-life trajectory datasets

5.1 Experimental Setting

Real-life Trajectory Datasets. We use four real-life datasets shown in Table 1 to test our solutions.

(1) **Taxi trajectory data**, referred to as **Taxi**, is the GPS trajectories collected by 12,727 taxis equipped with GPS sensors in Beijing during a period from Nov. 1, 2010 to Nov. 30, 2010. The sampling rate was one point per 60s, and **Taxi** has 39,100 data points on average per trajectory.

(2) **Truck trajectory data**, referred to as **Truck**, is the GPS trajectories collected by 10,368 trucks equipped with GPS sensors in China during a period from Mar. 2015 to Oct. 2015. The sampling rate varied from 1s to 60s. Trajectories mostly have around 50 to 90 thousand data points.

(3) **Service car trajectory data**, referred to as **SerCar**, is the GPS trajectories collected by a car rental company. We chose 11,000 cars from them, during Apr. 2015 to Nov. 2015. The sampling rate was one point per 3-5 seconds, and each trajectory has around 119.1K data points.

(4) **GeoLife trajectory data**, referred to as **GeoLife**, is the GPS trajectories collected in GeoLife project [25] by 182 users in a period from Apr. 2007 to Oct. 2011. These trajectories have a variety of sampling rates, among which 91% are logged in each 1-5 seconds or each 5-10 meters per point. The longest trajectory has 2,156,994 points.

Algorithms and implementation. We compared our algorithms OPERB and OPERB-A with two existing LS algorithms DP [6] and FBQS [12], and algorithms Raw-OPERB and Raw-OPERB-A, the counterparts of OPERB and OPERB-A without optimizations, respectively.

(1) Algorithm DP is a classic batch LS algorithm with an excellent compression ratio (shown in Figure 3).

(2) Algorithm FBQS is an online algorithm, and is the fastest existing LS algorithm (recall Section 2.2).

(3) Algorithm OPERB combines the algorithm in Figure 7 and the optimization techniques in Section 3.4, while algorithm Raw-OPERB is the basic algorithm in Figure 7 only.

(4) Algorithms OPERB-A and Raw-OPERB-A are the aggressive solutions extending OPERB and Raw-OPERB with trajectory interpolation, respectively.

All algorithms were implemented with Java. All tests were run on an x64-based PC with 4 Intel(R) Core(TM) i5-4570 CPU @ 3.20GHz and 16GB of memory, and each test was repeated over 3 times and the average is reported here.

5.2 Experimental Results

5.2.1 Evaluation of Compression Efficiency

In the first set of tests, we compare the efficiency (execution time) of our approaches OPERB and OPERB-A with algorithms DP and FBQS and with algorithms Raw-OPERB and Raw-OPERB-A. For fairness, we load and compress trajectories one by one, and only count the running time of the compressing process.

Exp-1.1: Impacts of the sizes of trajectories. To evaluate the impacts of the number of data points in a trajectory (i.e., the size of a trajectory), we chose 100 trajectories from **Taxi**, **Truck**, **SerCar** and **GeoLife**, respectively, and varied the size $|\vec{T}|$ of trajectories from 2,000 to 10,000, while fixed $\zeta = 40$ meters (m). The results are reported in Figure 12.

(1) Algorithms OPERB, OPERB-A and FBQS scale well with the increase of the size of trajectories on all datasets, and show a linear running time, while algorithm DP does not. This is consistent with their time complexity analyses.

(2) Algorithms OPERB and OPERB-A are the fastest LS algorithms, and are (3.8–5.3, 3.5–4.8, 4.6–7.2, 6.2–8.4) times faster than FBQS, and (9.6–17.6, 8.8–15.4, 8.4–16.3, 9.0–14.4) times faster than DP on (**Taxi**, **Truck**, **SerCar**, **GeoLife**), respectively. The running time of OPERB and OPERB-A is similar, and the difference is below 10%.

Exp-1.2: Impacts of the error bound ζ . To evaluate the impacts of ζ , we varied ζ from 10m to 100m on the entire **Taxi**, **Truck**, **SerCar** and **GeoLife**, respectively. The results are reported in Figure 13.

(1) All algorithms are not very sensitive to ζ , but their running time all decreases a little bit with the increase of ζ , as the increment of ζ decreases the number of directed line segments in the output. Further, algorithm DP is more sensitive to ζ than the other three algorithms.

(2) Algorithms OPERB and OPERB-A are obviously faster than DP and FBQS in all cases. OPERB is on average (13.9, 17.4, 14.7, 20.6) times faster than DP, and (4.1, 4.1, 5.4, 5.2) times faster than FBQS on (**Taxi**, **Truck**, **SerCar**, **GeoLife**), respectively. Algorithm OPERB-A is as fast as OPERB because trajectory interpolation is a light weight operation.

Exp-1.3: Impacts of optimization techniques. To evaluate the impacts of our optimization techniques (see Section 3.4), we compared algorithms OPERB and OPERB-A with Raw-OPERB and Raw-OPERB-A, respectively. We chose 500, 1000 and 500 trajectories from **Taxi**, **Truck**, **SerCar** and **GeoLife**, respectively, and varied ζ from 10m to 100m. The results are reported in Figure 14.

(1) The running time of all algorithms slightly decreases with the increase of ζ , consistent with Exp-1.2.

(2) The running time of Raw-OPERB is (85.0%, 79.6%, 90.4%, 100.4%) of OPERB on average on (**Taxi**, **Truck**, **SerCar**, **GeoLife**), respectively, and the running time of Raw-OPERB-A is (91.3%, 90.1%, 91.6%, 101.5%) of OPERB-A on average on (**Taxi**, **Truck**, **SerCar**, **GeoLife**), respectively. This shows that the optimization techniques have a limited impact on the efficiency of OPERB and OPERB-A. However, as will be shown immediately, the benefits of compression ratios are highly appreciated.

5.2.2 Evaluation of Compression Effectiveness

In the second set of tests, we compare the compression ratios of our algorithms OPERB and OPERB-A with DP and FBQS and with Raw-OPERB and Raw-OPERB-A, respectively. Given a set of trajectories $\{\vec{T}_1, \dots, \vec{T}_M\}$ and their piecewise line representations $\{\vec{T}_1, \dots, \vec{T}_M\}$, the compression ratio is $(\sum_{j=1}^M |\vec{T}_j|) / (\sum_{j=1}^M |\vec{T}_j|)$. Note that by the definition, algorithms with lower compression ratios are better.

Exp-2.1: Impacts of the error bound ζ . To evaluate the impacts of ζ on compression ratios of these algorithms, we varied ζ from 5m to 100m on the entire four datasets,

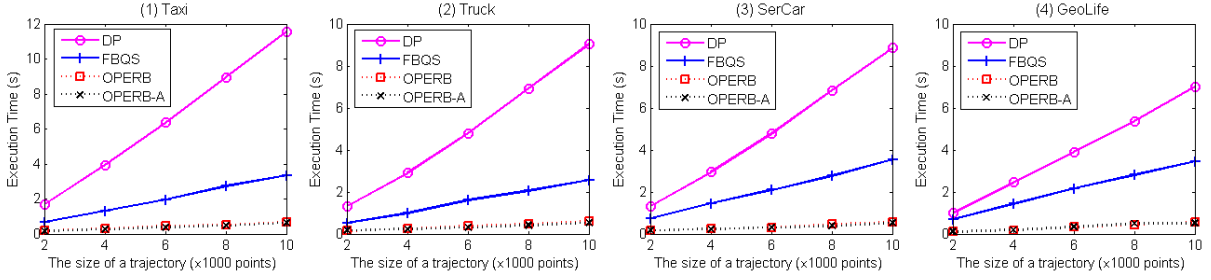


Figure 12: Efficiency evaluation: varying the size of trajectories.

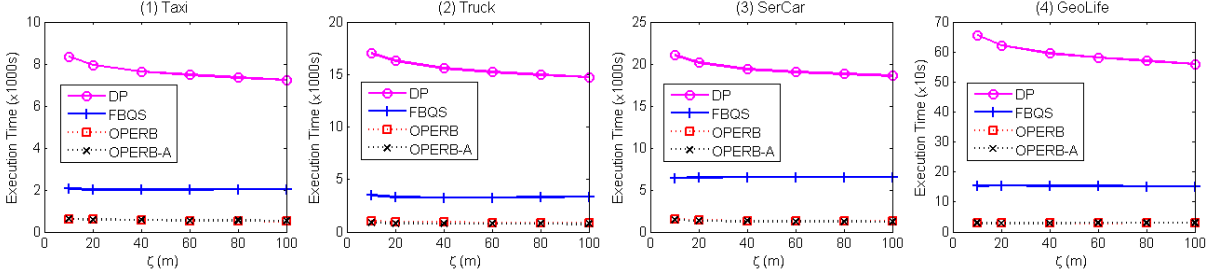


Figure 13: Efficiency evaluation: varying the error bound ζ .

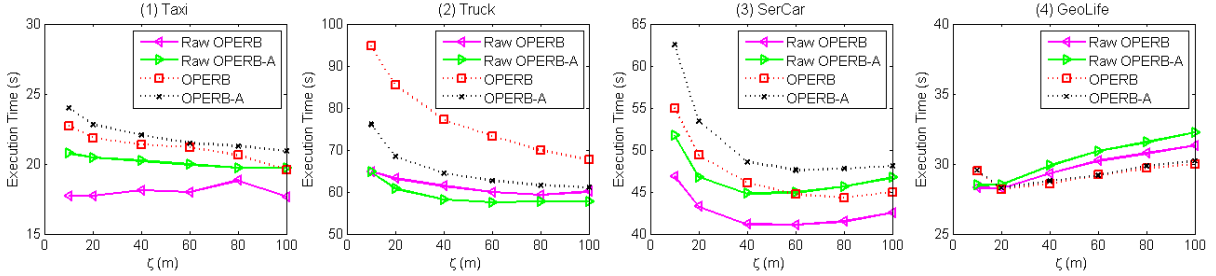


Figure 14: Efficiency evaluation: optimization techniques when varying the error bound ζ .

respectively. The results are reported in Figure 15.

(1) When increasing ζ , the compression ratios decrease. For example, in SerCar, the compression ratios are greater than 28.7% when $\zeta = 5m$, but are less than 6.6% when $\zeta = 100m$.

(2) GeoLife has the lowest compression ratios, compared with Taxi, Truck and SerCar, due to its highest sampling rate, Taxi has the highest compression ratios due to its lowest sampling rate, and Truck and SerCar have the compression ratios in the middle accordingly.

(3) First, algorithm OPERB has comparable compression ratios with FBQS and DP. For example, when $\zeta = 40m$, the compression ratios are (20.9%, 20.4%, 11.1%, 3.1%) of FBQS, (20.7%, 18.7%, 8.9%, 2.6%) of DP and (22.3%, 20.3%, 10.0%, 2.6%) of OPERB on (Taxi, Truck, SerCar, GeoLife), respectively. For all ζ , the compression ratios of OPERB are on average (107.2%, 98.3%, 92.9%, 85.1%) of FBQS and (107.7%, 106.6%, 113.5%, 99.6%) of DP on (Taxi, Truck, SerCar, GeoLife), respectively. OPERB is better than FBQS on Truck, SerCar and GeoLife, while a little worse on Taxi. The results also show that OPERB has a better performance than FBQS on datasets with high sampling rates.

Second, algorithm OPERB-A achieves the best compression ratios on all datasets and nearly all ζ values. Its compression ratios are on average (83.7%, 79.5%, 79.7%, 81.0%) of FBQS and (84.2%, 86.4%, 97.1%, 94.7%) of DP on (Taxi, Truck, SerCar, GeoLife), respectively. Similar to OPERB, OPERB-A has advantages on datasets with high sampling rates.

Exp-2.2: Impacts of the optimization techniques.

We compared algorithms OPERB and OPERB-A with Raw-OPERB and Raw-OPERB-A, respectively. We varied ζ from 5m to 100m on the entire Taxi, Truck, SerCar and GeoLife, respectively. The results are reported in Figure 16.

(1) The optimizations have great impacts on the compression ratios of OPERB and OPERB-A. Indeed, OPERB is on average (87.9%, 71.8%, 61.8%, 58.0%) of Raw-OPERB, and OPERB-A is on average (93.1%, 88.5%, 77.1%, 78.5%) of Raw-OPERB-A on (Taxi, Truck, SerCar, GeoLife), respectively. Note that the optimization techniques have a better impact on datasets with high sampling rates.

(2) The impacts of the optimization techniques increase with the increase of ζ on Taxi and Truck. For example, OPERB is (92.1%, 87.3%, 82.6%) of Raw-OPERB on Taxi, and (78.5%, 70.9%, 63.7%) of Raw-OPERB on Truck when $\zeta = (10, 40, 100)$, respectively. It is similar for algorithm OPERB-A.

Exp-2.3: Distribution of line segments.

To further evaluate the difference of the compression results of these algorithms, we chose 100 trajectories from each of (Taxi, Truck, SerCar, GeoLife), while fixed $\zeta = 40m$. For a $\overline{\mathcal{T}} = (\mathcal{L}_1, \mathcal{L}_2, \dots, \mathcal{L}_M)$ derived from trajectories by a compression algorithm, we count the number of points, C_i , included in each \mathcal{L}_i , then let $\mathcal{Z}(k) = |\{C_i | C_i = k\}|$, i.e., $\mathcal{Z}(5)$ means the number of all \mathcal{L}_i containing 5 data points. Note that the start/end points are repeatedly counted for adjacent line segments, and, hence, there may be some lines having only

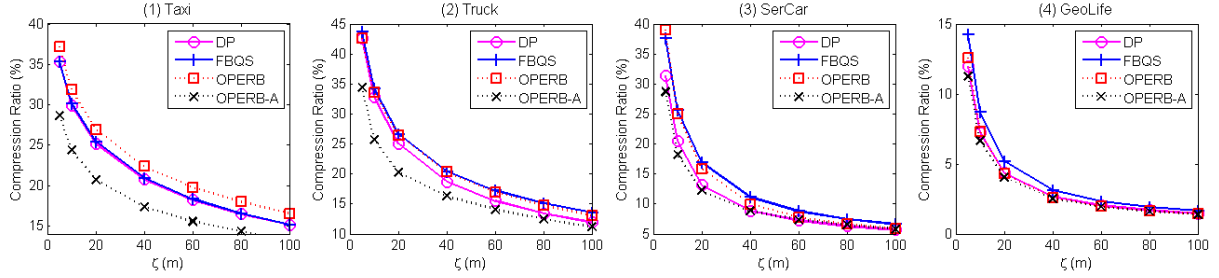


Figure 15: Effectiveness evaluation: varying the error bound ζ .

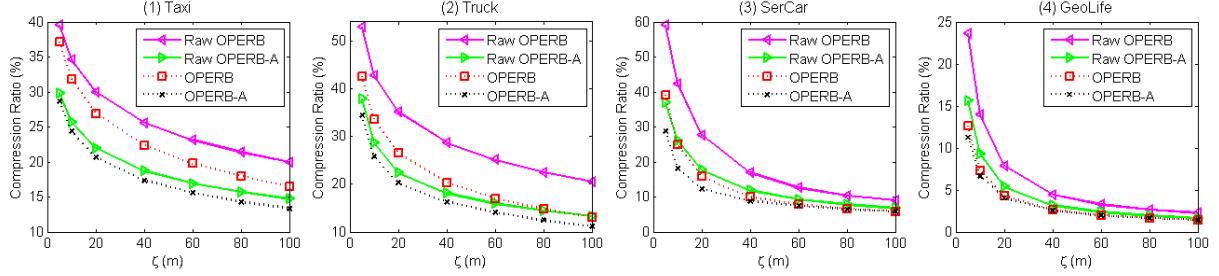


Figure 16: Effectiveness evaluation: optimization techniques when varying the error bound ζ .

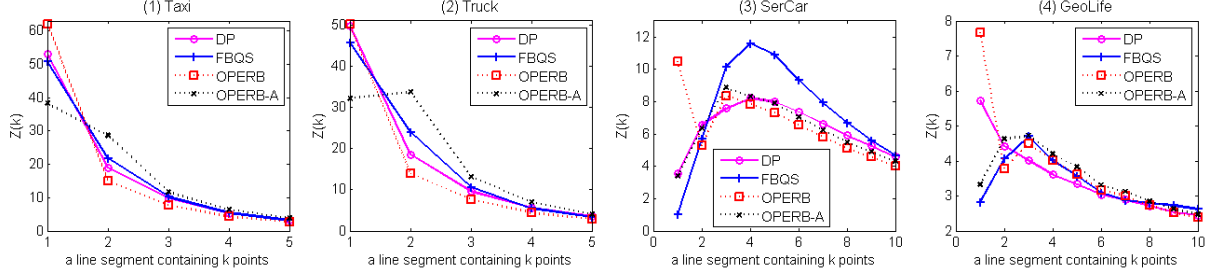


Figure 17: Effectiveness evaluation: distribution of line segments. The horizontal coordinate is the number k of data points, and the vertical coordinate is the number $Z(k)$ of line segments containing k points.

one point. The results are reported in Figure 17.

(1) Algorithms OPERB-A and DP produce more line segments containing large number of points (heavy line segments) than FBQS and OPERB. Heavy line segments are closely related to compression ratios, and help to decrease compression ratios. The distribution of line segments is consistent with the compression ratios shown above.

(2) Algorithm OPERB has the largest number of line segments containing only one point. However, they are reduced by OPERB-A to a large extent.

5.2.3 Evaluation of Average Errors

In the third set of tests, we evaluate the average errors of these algorithms. We varied ζ from 5m to 100m on the entire Taxi, Truck, SerCar and GeoLife, respectively. Given a set of trajectories $\{\vec{T}_1, \dots, \vec{T}_M\}$ and their piecewise line representations $\{\vec{T}_1, \dots, \vec{T}_M\}$, and point $P_{j,i}$ denoting a point in trajectory \vec{T}_j contained in a line segment $\mathcal{L}_{l,i} \in \vec{T}_l$ ($l \in [1, M]$), then the average error is $\sum_{j=1}^M \sum_{i=0}^M d(P_{j,i}, \mathcal{L}_{l,i}) / \sum_{j=1}^M |\vec{T}_j|$. The results are reported in Figure 18.

(1) Average errors obviously increase with the increase of ζ . Taxi also has the lowest average errors than Truck and SerCar for all algorithms, as it has the highest compression ratios, and SerCar has the highest average errors, as it has the lowest compression ratios among the three datasets.

(2) Algorithm DP not only has better compression ratios,

but also has lower average errors than algorithm FBQS on all datasets and most ζ values.

(3) Algorithms OPERB and OPERB-A have similar average errors with each other. Meanwhile, OPERB-A does not introduce extra error. Compared with DP and FBQS, their errors are a little smaller on Taxi and a little larger on SerCar.

5.2.4 Evaluation of Trajectories Interpolation

In the last set of tests, we evaluate the lazy trajectory interpolation policy of algorithm OPERB-A.

Exp-4.1: Patching ratios. To evaluate the patching ratios of OPERB-A and the impacts of ζ on patching ratios, we varied ζ from 10m to 100m, while fixed $\gamma_m = \pi/3$, on Taxi, Truck, SerCar and GeoLife, respectively. The patching ratio is defined as $\frac{N_p}{N_a} * 100\%$, where N_p is the number of patching points successful added to the trajectories, and N_a is the number of anonymous line segments before trajectory interpolation. The results are reported in Figure 19–(1).

(1) The patching ratios are on average (50.5%, 60.3%, 63.2%, 51.5%) on (Taxi, Truck, SerCar, GeoLife), respectively. That is, more than half of the anomalous line segments are successfully eliminated by the lazy trajectory output policy.

(2) The patching ratios on Taxi, Truck, SerCar and GeoLife decrease from $\zeta = 30m$ or $\zeta = 40m$, respectively.

(3) Taxi has the lowest patching ratios due to its relatively

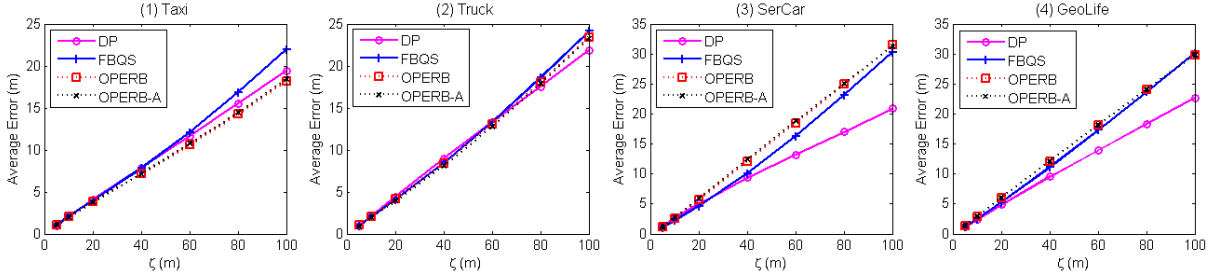


Figure 18: Evaluation of average errors: varying the error bound ζ .

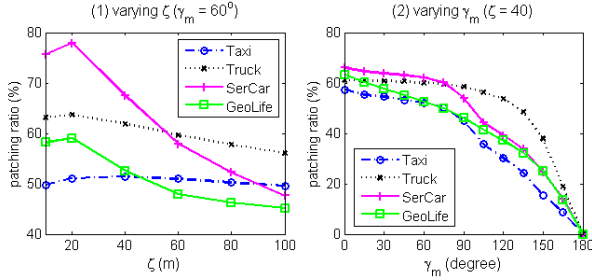


Figure 19: Patching ratios of OPERB-A.

lower sampling rate. Moreover, the number of anomalous line segments output by OPERB-A is significantly less than the other algorithms. That is, even a patching ratio like 50.5% is enough to improve the compression ratio and to make OPERB-A have the best compression ratio.

Exp-4.2: Impacts of γ_m for trajectory interpolation. Our trajectory interpolation uses a parameter $\gamma_m \in [0, \pi]$ to restrict the included angle of two line segments. Note that a smaller γ_m means that a larger direction change is allowed in trajectory interpolation. To evaluate the impacts of γ_m on patching ratios, we randomly chose 100 trajectories from each of (Taxi, Truck, SerCar), and we varied γ_m from 0° to 180° (or 0 to π), while fixed $\zeta = 40m$. The results are reported Figure 19–(2).

(1) When varying γ_m , the patching ratio decreases with the increase of γ_m . The patching ratio decreases (a) slowly when $\gamma_m \in [0, 75^\circ]$, (b) fast when $\gamma_m \in (75^\circ, 145^\circ)$, and (c) fastest when $\gamma_m \in (145^\circ, 180^\circ]$. The region $[30^\circ, 90^\circ]$ is the candidate region for γ_m with both high patching ratios and reasonable patch points, not too far away from the points P_{s+k} and P_{s+k+1} , between which the patch point is interpolated. Hence, we set $\gamma_m = \pi/3$ by default.

(2) Parameter γ_m has different impacts on different data sets. The patching ratio of Taxi decreases quickly when $\gamma_m \in [80^\circ, 120^\circ]$, it is the result of taxis running on urban road networks, which have more crossroads. The patching ratio of Truck decreases slowly in this region because many trucks are running in suburban districts or between cities, in which there are less crossroads.

Summary. From these tests we find the following.

(1) *Efficiency.* OPERB and OPERB-A are the fastest algorithms, which are on average (13.9, 17.4, 14.7, 20.6) times faster than DP, and (4.1, 4.1, 5.4, 5.2) times faster than FBQS on (Taxi, Truck, SerCar, GeoLife), respectively.

(2) *Compression ratios.* (a) OPERB is comparable with FBQS and DP. Its compression ratios are on average (107.2%, 98.3%, 92.9%, 85.1%) of FBQS and (107.7%,

106.6%, 113.5%, 99.6%) of DP on (Taxi, Truck, SerCar, GeoLife), respectively, and OPERB has a better performance on trajectories with higher sampling rates. (b) OPERB-A has the best compression ratios on all datasets and nearly all ζ values. Its compression ratios are on average (83.7%, 79.5%, 79.7%, 81.0%) of FBQS and (84.2%, 86.4%, 97.1%, 94.7%) of DP on (Taxi, Truck, SerCar, GeoLife), respectively. It shows its advantage on trajectories with both high and low sampling rates. (c) The optimization techniques are effective for algorithms OPERB and OPERB-A on all datasets.

(3) *Average errors.* Algorithm OPERB has similar average errors with OPERB-A. They have lower average errors than the other algorithms on Taxi while higher on SerCar.

(4) *Patching ratios.* OPERB-A successfully eliminates more than a half of anomalous line segments by patching data points, which improves the compression ratio, and indeed makes it achieve the best compression ratio.

6. RELATED WORK

Trajectory compression algorithms are normally classified into two categories, namely lossless compression and lossy compression [18]. (1) Lossless compression methods enable exact reconstruction of the original data from the compressed data without information loss. For example, delta compression [19] is a lossless compression technique, which has zero error and a time complexity of $O(n)$, where n is the number of data points in a trajectory. The limitation of lossless compression lies in that its compression ratio is relatively poor [19]. (2) In contrast, lossy compression methods allow errors or derivations, compared with the original trajectories. These techniques typically identify important data points, and remove statistical redundant data points from a trajectory, or replace original data points in a trajectory with other places of interests, such as roads and shops. They focus on good compression ratios with acceptable errors, and a large number of lossy trajectory compression techniques have been developed. In this work we focus on lossy compression of trajectory data,

We next introduce the related work on lossy trajectory compression from two aspects: line simplification based methods and semantics based methods.

Line simplification based methods. Line simplification based methods not only have good compression ratios and deterministic error bounds, but also are easy to implement (see an evaluation report [23]). Hence, they are widely used in practice, even for freely moving objects without the restriction of road networks. And according to the way they process trajectories, they are further divided into batch processing and online processing methods [19].

(1) Batch algorithms require that all trajectory points must

be loaded before they start compressing. Batch algorithms can be either top-down or bottom-up. Top-down algorithms recursively divide a trajectory into sub-trajectories until the stopping condition is met [11]. The DP algorithm [6] is the most classic top-down approach, and [15] improves DP with the synchronous Euclidean distance, instead of the Euclidean distance. Bottom-up algorithms [3, 11] are the natural complement to top-down ones, which recursively merge adjacent sub-trajectories with the smallest distance, initially $n/2$ sub-trajectories for a trajectory with n points, until the stopping condition is met. Note that the distances of newly generated line segments are recalculated during the process. (2) Online algorithms do not need to have the entire trajectory ready before they start compressing, and are appropriate for compressing trajectories on sensors of mobile devices. Existing online algorithms [11, 15, 18] usually use a fixed or open window and compress sub-trajectories in the window.

However, these existing online algorithms are not one-pass. In this study, we propose a novel local distance checking method, based on which we develop one-pass online algorithms that are totally different from the window based algorithms. Further, as shown in the experimental study, our approaches are clearly superior to the existing online algorithms, in terms of both efficiency and effectiveness.

Semantics based methods. The trajectories of certain moving objects such as cars and trucks are constrained by road networks. These moving objects typically travel along road networks, instead of the line segment between two points. Trajectory compression methods based on road networks [4, 5, 7, 9, 20, 24] project trajectory points onto roads (also known as Map-Matching). Moreover, [7, 24] mines and uses high frequency patterns of compressed trajectories, instead of roads, to further improve compression effectiveness. Some methods [21, 22] compress trajectories beyond the use of road networks, which further make use of other user specified domain knowledge, such as places of interests along the trajectories [21]. There are also compression algorithms preserving the direction of the trajectory [13, 14].

These approaches are orthogonal to line simplification based methods, and may be combined with each other to further improve the effectiveness of trajectory compression.

7. CONCLUSIONS AND FUTURE WORK

We have proposed OPERB and OPERB-A, two one-pass error bounded trajectory simplification algorithms. First, we have developed a novel local distance checking approach, based on which we then have designed OPERB, together with optimization techniques for improving its compression ratio. Second, by allowing interpolating new data points into a trajectory under certain conditions, we have developed an aggressive one-pass error bounded trajectory simplification algorithm OPERB-A, which has significantly improved the compression ratio. Finally, we have experimentally verified that both OPERB and OPERB-A are much faster than FBQS, the fastest existing LS algorithm, and in terms of compression ratio, OPERB is comparable with DP, and OPERB-A is better than DP on average, the existing LS algorithm with the best compression ratio.

A couple of issues need further study. We are to incorporate semantic based methods and to study alternative forms of fitting functions to further improve the effectiveness of trajectory compression.

8. REFERENCES

- [1] Full version. <http://mashuai.buaa.edu.cn/OPERB-full.pdf>.
- [2] H. Cao, O. Wolfson, and G. Trajcevski. Spatio-temporal data reduction with deterministic error bounds. *VLDB J.*, 15(3):211–228, 2006.
- [3] M. Chen, M. Xu, and P. Franti. A fast multiresolution polygonal approximation algorithm for GPS trajectory simplification. *TIP*, 21(5):2770–2785, 2012.
- [4] Y. Chen, K. Jiang, Y. Zheng, C. Li, and N. Yu. Trajectory simplification method for location-based social networking services. In *GIS-LBSN*, 2009.
- [5] A. Civilis, C. S. Jensen, and S. Pakalnis. Techniques for efficient road-network-based tracking of moving objects. *TKDE*, 17(5):698–712, 2005.
- [6] D. H. Douglas and T. K. Peucker. Algorithms for the reduction of the number of points required to represent a digitized line or its caricature. *The Canadian Cartographer*, 10(2):112–122, 1973.
- [7] R. Gotsman and Y. Kanza. A dilation-matching-encoding compaction of trajectories over road networks. In *GeoInformatica*, 2015.
- [8] J. Hershberger and J. Snoeyink. Speeding up the douglas-peucker line-simplification algorithm. *Technical Report*, University of British Columbia, 1992.
- [9] C. C. Hung, W. Peng, and W. Lee. Clustering and aggregating clues of trajectories for mining trajectory patterns and routes. *VLDB J.*, 24(2):169–192, 2015.
- [10] S. Kaul, M. Gruteser, V. Rai, and J. Kenney. On predicting and compressing vehicular GPS traces. In *Vehi-Mobi*, 2010.
- [11] E. J. Keogh, S. Chu, D. M. Hart, and M. J. Pazzani. An online algorithm for segmenting time series. In *ICDE*, 2001.
- [12] J. Liu, K. Zhao, P. Sommer, S. Shang, B. Kusy, and R. Jurdak. Bounded quadrant system: Error-bounded trajectory compression on the go. In *ICDE*, 2015.
- [13] C. Long, R. C.-W. Wong, and H. Jagadish. Direction-preserving trajectory simplification. *PVLDB*, 6(10):949–960, 2013.
- [14] C. Long, R. C.-W. Wong, and H. Jagadish. Trajectory simplification: on minimizing the direction-based error. *PVLDB*, 8(1):49–60, 2014.
- [15] N. Meratnia and R. A. de By. Spatiotemporal compression techniques for moving point objects. In *EDBT*, 2004.
- [16] R. Metha and V.K.Mehta. *The Principles of Physics for 11*. S Chand, 1999.
- [17] J. S. B. Mitchell, V. Polishchuk, and M. Sysikaski. Minimum-link paths revisited. *Computational Geometry*, 47(6):651–667, 2014.
- [18] J. Muckell, P. W. Olsen, J.-H. Hwang, C. T. Lawson, and S. S. Ravi. Compression of trajectory data: a comprehensive evaluation and new approach. *GeoInformatica*, 18(3):435–460, 2014.
- [19] A. Nibali and Z. He. Trajic: An effective compression system for trajectory data. *TKDE*, 27(11):3138–3151, 2015.
- [20] I. S. Popa, K. Zeitouni, VincentOria, and A. Kharrat. Spatio-temporal compression of trajectories in road networks. *GeoInformatica*, 19(1):117–145, 2014.
- [21] K.-F. Richter, F. Schmid, and P. Laube. Semantic trajectory compression: Representing urban movement in a nutshell. *J. Spatial Information Science*, 4(1):3–30, 2012.
- [22] F. Schmid, K. Richter, and P. Laube. Semantic trajectory compression. In *SSTD*, 2009.
- [23] W. Shi and C. Cheung. Performance evaluation of line simplification algorithms for vector generalization. *Cartographic Journal*, 43(1):27–44, 2006.
- [24] R. Song, W. Sun, B. Zheng, and Y. Zheng. PRESS: A novel framework of trajectory compression in road networks. *PVLDB*, 7(9):661–672, 2014.
- [25] Y. Zheng, X. Xie, and W. Ma. GeoLife: A collaborative social networking service among user, location and trajectory. *IEEE Data Eng. Bull.*, 33(2):32–39, 2010.

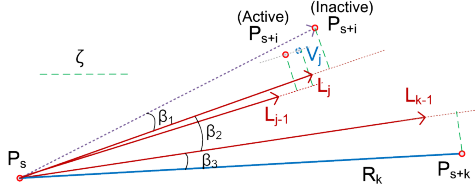


Figure 20: Example for the proof of Theorem 2

Appendix A: Detailed Proofs

A.1 Proof of Lemma 3

By the revised fitting function \mathbb{F}' for a stepwise sub-trajectory and $d(P_{s+i}, \mathcal{L}_{i-1}) \leq \zeta/2$ for all $i \in [2, k]$, we have $\Delta\theta \leq \sum_{i=2}^k \frac{1}{i} * \arcsin(\frac{1}{i})$, which is monotonically increasing with the increment of k .

As $x \leq \arcsin(x) \leq \frac{x}{\sqrt{1-x^2}}$ ($0 \leq x < 1$), we have $\frac{1}{i} \leq \arcsin \frac{1}{i} \leq \frac{1}{\sqrt{i^2-1}}$ ($i \geq 2$), from which we have the following.

$$(1) \Delta\theta \geq \lim_{k \rightarrow \infty} \sum_{i=2}^k \frac{1}{i^2} = \pi^2/6 - 1 \approx 0.6449, \text{ and}$$

$$(2) \Delta\theta \leq \lim_{k \rightarrow \infty} \sum_{i=2}^k \left(\frac{1}{i} * \frac{1}{\sqrt{i^2-1}} \right) \\ < \int_2^\infty \left(\frac{1}{x} * \frac{1}{\sqrt{x^2-1}} \right) dx + \frac{1}{2} * \frac{1}{\sqrt{2^2-1}} \\ = \frac{\pi}{6} + \frac{1}{2\sqrt{3}} \approx 0.8123.$$

From these, we have the conclusion. \square

A.2 Proof of Lemma 4

Consider the four directed line segments $\mathcal{R}_i = \overrightarrow{P_s P_{s+i}}$, $\mathcal{R}_k = \overrightarrow{P_s P_{s+k}}$, \mathcal{L}_{i-1} and \mathcal{L}_{k-1} shown in Figure 6 by Lemma 3. Further, let $\beta_1 = \mathcal{R}_i.\theta - \mathcal{L}_{i-1}.\theta$, $\beta_2 = \mathcal{L}_{k-1}.\theta - \mathcal{L}_i.\theta$, $\beta_3 = \mathcal{R}_k.\theta - \mathcal{L}_{k-1}.\theta$. We then adjust the included angles β_1 as follows:

- (a) if $\pi/2 < |\beta_1| \leq \pi$, then $\beta_1 = \pi - \beta_1$,
- (b) if $\pi < |\beta_1| \leq \frac{3}{2}\pi$, then $\beta_1 = \beta_1 - \pi$,
- (c) if $\frac{3}{2}\pi < |\beta_1| \leq 2\pi$, then $\beta_1 = 2\pi - \beta_1$, and
- (d) $\beta_1 = |\beta_1|$, otherwise.

The included angle β_2 is bounded by Lemma 3, and the included angle β_3 is adjusted along the same line as β_1 .

Observe that $d(P_{s+i}, \mathcal{R}_k) \leq i * \frac{\zeta}{2} * \sin(|\beta_1| + |\beta_2| + |\beta_3|) \leq i * \frac{\zeta}{2} * \sin(\arcsin(\frac{1}{i}) + \sum_{j=i+1}^{k-1} (\frac{1}{j} * \arcsin \frac{1}{j}) + \arcsin(\frac{1}{k}))$.

(1) We first show that $\arcsin(\frac{1}{i}) + \sum_{j=i+1}^{k-1} (\frac{1}{j} * \arcsin \frac{1}{j}) + \arcsin(\frac{1}{k})$ falls in $(0, \frac{\pi}{2})$.

The distance $d(P_{s+i}, \mathcal{R}_k)$ is monotonically increasing *w.r.t.* k when fixing i . Let $g(k) = \sum_{j=i+1}^{k-1} (\frac{1}{j} * \arcsin \frac{1}{j}) + \arcsin(\frac{1}{k})$, and it suffices to show that $g(k+1) - g(k) \geq 0$, which is shown below.

$$g(k+1) - g(k) = \frac{1}{k} * \arcsin \frac{1}{k} + \arcsin \frac{1}{k+1} - \arcsin \frac{1}{k} \\ \geq \frac{1}{k} * \frac{1}{k} + \frac{1}{k+1} - \frac{1}{\sqrt{k^2-1}} > 0.$$

When $i \geq 2$, we have the following.

$$\arcsin \frac{1}{i} + \sum_{j=i+1}^{k-1} (\frac{1}{j} * \arcsin \frac{1}{j}) + \arcsin \frac{1}{k} \\ \leq \arcsin(\frac{1}{i}) + \sum_{j=i+1}^\infty (\frac{1}{j} * \arcsin \frac{1}{j}) \\ \leq \arcsin(\frac{1}{2}) + \sum_{j=3}^\infty (\frac{1}{j} * \arcsin \frac{1}{j}) \\ \approx 1.0741 = 61.54^\circ.$$

(2) For $k \leq 4 \times 10^5$, we have $i * \sin(|\beta_1| + |\beta_2| + |\beta_3|) < 2$, and, hence, we have $d(P_{s+i}, \mathcal{R}_k) < \frac{\zeta}{2} * 2 = \zeta$.

This completes the proof.

A.3 Proof of Theorem 2

We only need to consider those points P_{s+i} such that $|P_s P_{s+i}| > \zeta$ (otherwise, it is obvious that $d(P_{s+i}, \mathcal{R}_k) \leq \zeta$).

(1) First consider inactive points P_{s+i} that are mapped to a virtual point V_{j_i} in \vec{T}_v ($j_i \geq 2$). (2) Then consider active points P_{s+i} that are mapped to a virtual point V_{j_i} in \vec{T}_v ($j_i = \lceil (|\mathcal{R}_i| * 2 / \zeta - 0.5) \rceil$). We assume that P_{s+k} is an active point and $j_k > j_i$.

Then $d(P_{s+i}, \mathcal{R}_k) = |\mathcal{R}_i| * \sin(|\beta_1| + |\beta_2| + |\beta_3|)$, where β_1, β_2 and β_3 are the included angles between V_{j_i} and P_{s+i} , between V_{j_i} and V_{j_k} and between V_{j_k} and P_{s+k} that are adjusted along the same lines as the proof of Lemma 4, as shown in Figure 20. Note that here $\beta_1 \leq \frac{\zeta}{4} / (j_i * \frac{\zeta}{2}) = \arcsin \frac{1}{2j_i}$ and $\beta_3 \leq \frac{\zeta}{4} / (j_k * \frac{\zeta}{2}) = \arcsin \frac{1}{2j_k}$. Along the same lines as the proof of Lemma 4, we have the following.

$$d(P_{s+i}, \mathcal{R}_k) \text{ (when } i \geq 2 \text{ and } k \leq 4 \times 10^5) \\ \leq \frac{\zeta}{2} * (j_i + \frac{1}{2}) * \sin(\arcsin \frac{1}{2j_i} + \arcsin \frac{1}{2j_k} + \arcsin \sum_{i=j_i+1}^{j_k-1} \frac{1}{i} * \arcsin \frac{1}{i}) \leq \zeta.$$

Appendix B: Extended Experimental Study

To evaluate the number of anomalous line segments in the output line segments of OPERB, we varied ζ from 10m to 100m on Taxi, Truck, SerCar and GeoLife, respectively. The results are reported in Figure 21.

Figure 21(1) is the number of line segments with at most two active points (may have inactive points), and Figure 21(2) is the number of line segments with two points (both are active points, without any inactive points). More than 40% of line segments in Taxi and Truck and more than 10% when $\zeta \leq 40$ in SerCar are anomalous line segments. Hence, the compression ratio can be significantly improved if anomalous line segments could (partially) be eliminated.

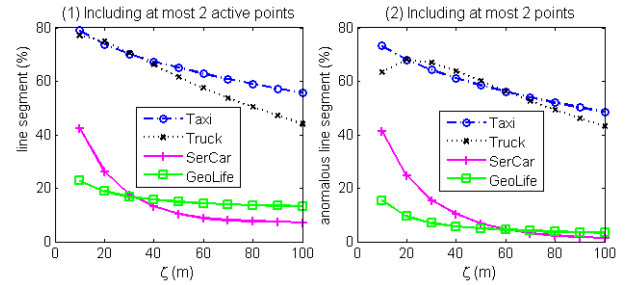


Figure 21: The distribution of line segments of OPERB (varying ζ).

Appendix C: P-codes of Algorithm OPERB-A

Figure 22 is the p-codes of algorithm OPERB-A, which expands OPERB majorly in two folders:

(1) It defines a procedure, $\text{patch}(\mathcal{R}_{pre}, \mathcal{R}_{ano}, \mathcal{R}_{suc}, \zeta, \gamma_m)$, to eliminate anomalous line segments. The procedure $\text{patch}()$ takes as input the preview line segment \mathcal{R}_{pre} , the anomalous line segment \mathcal{R}_{ano} , the current line segment \mathcal{R}_{suc} , the error bound ζ and the maximum included angle γ_m . It returns a triple $(\mathcal{R}_a, \mathcal{R}_b, \text{flag})$, where \mathcal{R}_a and \mathcal{R}_b are two line segments and flag denotes whether the anomalous line segment is successful eliminated or not. If there exists a patch point G *w.r.t.* \mathcal{R}_{ano} between \mathcal{R}_{pre} and \mathcal{R}_{suc} (satisfying the three conditions mentioned in the patch method of Section 4.1. Note the parameters ζ and γ_m are needed in

Algorithm OPERB – A($\vec{T}[P_0, \dots, P_n], \zeta, \gamma_m$)

```
1.  $\vec{T} := \emptyset$ ;  $P_e := P_0$ ;  $\mathcal{R}_{pre} := \text{nil}$ ;  $\mathcal{R}_{ano} := \text{nil}$ ;  
   ( $P_a, \text{flag}$ ) := getActivePoint( $\vec{T}, P_0, P_0, \mathcal{L}_0, \zeta$ );  
2. while  $P_a \neq \text{nil}$  do  
3.    $P_s := P_e$ ;  $\mathcal{L}_a = \mathbb{F}(P_a, \overrightarrow{P_s P_s})$ ;  
4.   ( $P_a, \text{flag}$ ) := getActivePoint( $\vec{T}, P_s, P_a, \mathcal{L}_a, \zeta$ );  
5.   while  $P_a \neq \text{nil} \ \& \ \text{flag} = \text{true}$  do  
6.      $\mathcal{L}_a := \mathbb{F}(P_a, \mathcal{L}_a)$ ;  $P_e := P_a$ ;  
7.     ( $P_a, \text{flag}$ ) := getActivePoint( $\vec{T}, P_s, P_a, \mathcal{L}_a, \zeta$ );  
8.     if  $P_a \neq \text{nil} \ \& \ \mathcal{R}_{ano} = \text{nil} \ \& \ (P_s P_e \text{ only having 2 points})$  then  
        $\mathcal{R}_{ano} := \overrightarrow{P_s P_e}$ ;  
9.     if  $P_a \neq \text{nil} \ \& \ \mathcal{R}_{ano} \neq \text{nil} \ \& \ \mathcal{R}_{ano} \neq \overrightarrow{P_s P_e}$  then  
10.      ( $\mathcal{R}_a, \mathcal{R}_b, \text{flag}$ ) = patch( $\mathcal{R}_{pre}, \mathcal{R}_{ano}, \overrightarrow{P_s P_e}, \zeta, \gamma_m$ );  
11.      if  $\text{flag} = \text{true}$  then  $\vec{T} := \vec{T} \cup \{\mathcal{R}_a\}$ ;  $\mathcal{R}_{pre} := \mathcal{R}_b$ ;  
12.      else  $\vec{T} := \vec{T} \cup \{\mathcal{R}_{pre}, \mathcal{R}_{ano}\}$ ;  $\mathcal{R}_{pre} := \overrightarrow{P_s P_e}$ ;  
13.       $\mathcal{R}_{ano} := \text{nil}$ ;  
14.      else if  $P_a \neq \text{nil} \ \& \ \mathcal{R}_{ano} = \text{nil}$  then  
15.         $\vec{T} := \vec{T} \cup \{\mathcal{R}_{pre}\}$ ;  $\mathcal{R}_{pre} := \overrightarrow{P_s P_e}$ ;  
16.       $\vec{T} := \vec{T} \cup \{\mathcal{R}_{pre}, \mathcal{R}_{ano}\}$ ;  
17. return  $\vec{T}$ .
```

Procedure **getActivePoint**($\vec{T}, P_s, P_a, \mathcal{L}_a, \zeta$)

```
1.  $i := a + 1$ ;  $\text{flag} := \text{true}$ ;  
2. while ( $(|\mathcal{R}_i| - |\mathcal{L}_a|) \leq \zeta/4 \ \& \ i \leq n \ \& \ (i - s) \leq 4 \times 10^5$ ) do {  
3.   if  $d(P_i, \mathcal{L}_a) > \zeta/2$  or  $d(P_i, \mathcal{R}_a) > \zeta$  then  
4.      $\text{flag} := \text{false}$ ; break ;  
5.    $i := i + 1$ ; }  
6. if  $d(P_i, \mathcal{L}_a) > \zeta/2 \ \& \ |\mathcal{L}_a| > 0$  then  $\text{flag} := \text{false}$ ;  
7. if  $i = n + 1$  then  $P_i := \text{nil}$ ;  
8. return ( $P_i, \text{flag}$ ).
```

Procedure **patch**($\mathcal{R}_{pre}, \mathcal{R}_{ano}, \mathcal{R}_{suc}, \zeta, \gamma_m$)

```
1. if  $\mathcal{R}_{pre} = \text{nil}$  then return ( $\text{nil}, \text{nil}, \text{false}$ );  
2. if exists a patch point  $G$  w.r.t.  $\mathcal{R}_{ano}$  Then  
3.   return ( $(\mathcal{R}_{pre}, P_s)G, G(\mathcal{R}_{suc}, P_e), \text{true}$ );  
4. else return ( $\text{nil}, \text{nil}, \text{false}$ ).
```

Figure 22: P-codes of algorithm OPERB-A.

this step), then it returns $(\overrightarrow{(\mathcal{R}_{pre}, P_s)G}, \overrightarrow{G(\mathcal{R}_{suc}, P_e)}, \text{true})$ (line 2). Otherwise, it returns ($\text{nil}, \text{nil}, \text{false}$) (lines 1, 3).

(2) It expands the line 8 of algorithm OPERB to the lines 8-16 of algorithm OPERB-A. It first marks an anomalous line segment as \mathcal{R}_{ano} (line 8). Then it patches the anomalous line segment by calling **patch**($\mathcal{R}_{pre}, \mathcal{R}_{ano}, \overrightarrow{P_s P_e}, \zeta, \gamma_m$), which returns $(\mathcal{R}_a, \mathcal{R}_b, \text{flag})$, in the next loop. It outputs \mathcal{R}_a and marks \mathcal{R}_b as \mathcal{R}_{pre} when the patching is succeed

($\text{flag} = \text{true}$), or outputs \mathcal{R}_{pre} and \mathcal{R}_{ano} , and marks the current line segment $\overrightarrow{P_s P_e}$ as \mathcal{R}_{pre} when it is failed ($\text{flag} = \text{false}$) (lines 9-13). If there is no anomalous line segment, then OPERB-A directly outputs \mathcal{R}_{pre} and marks the current line segment $\overrightarrow{P_s P_e}$ as \mathcal{R}_{pre} (lines 14-15). At last, OPERB-A outputs the last \mathcal{R}_{pre} and the last \mathcal{R}_{ano} (line 16).

Algorithm OPERB-A is one-pass and error bounded. It takes $O(1)$ space, the same as OPERB, as the directed line segment in \vec{T} can be output immediately once it is generated.

Appendix D: Cases Study

In this set of tests, we show that the trajectory interpolation and lazy point output policy adopted by algorithm OPERB-A produces reasonable results with cases study.

We fixed $\zeta = 40m$ in these cases.

Case (1): An Example on Taxi Trajectories

Figure 23(a) is an example sub-trajectory with 35 points collected from a taxi in Beijing, China on Taxi, whose data points are marked as black solid dots on the map. The compressed results by DP, FBQS, OPERB, OPERB-A with $\gamma_m = 180^\circ$ and OPERB-A with $\gamma_m = 60^\circ$ are shown in Figure 23(b), Figure 23(c), Figure 23(d), Figure 23(e) and Figure 23(f), respectively, and have 19, 20, 20, 20 and 17 data points, respectively. Note that $\gamma_m = 60^\circ$ is the default setting and $\gamma_m = 180^\circ$ means that no patch points are allowed to be interpolated into a trajectory. Among those seven anomalous line segments of OPERB-A (Figure 23(e)), three of them are replaced by patch points.

Case (2): An Example on Truck Trajectories

Figure 24(a) is an example sub-trajectory with 139 points collected from a truck in Guangxi, China on Truck, whose data points are marked as black solid dots on the map. The compressed results by DP, FBQS, OPERB, OPERB-A with $\gamma_m = 180^\circ$ and OPERB-A with $\gamma_m = 60^\circ$ are shown in Figure 24(b), Figure 24(c), Figure 24(d), Figure 24(e) and Figure 24(f), respectively, and have 26, 26, 25, 25 and 18 data points, respectively. Among those twelve anomalous line segments, seven of them are replaced by patch points.

Remark. Note in these two cases on (Taxi, Truck), respectively, the anomalous line segments and patch points are manually marked in the pictures, and carefully checked. We find that those patch points are very reasonable, as shown in Figures 23(f) and 24(f).

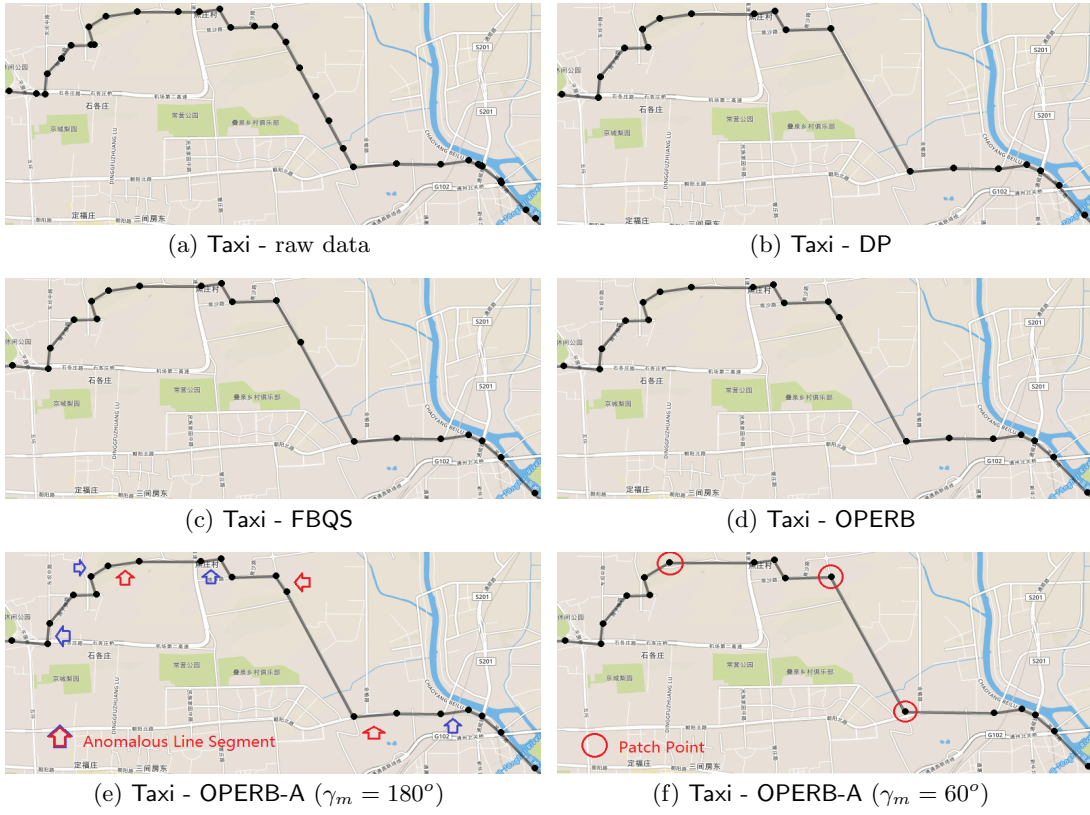


Figure 23: An Example on Taxi Trajectories.

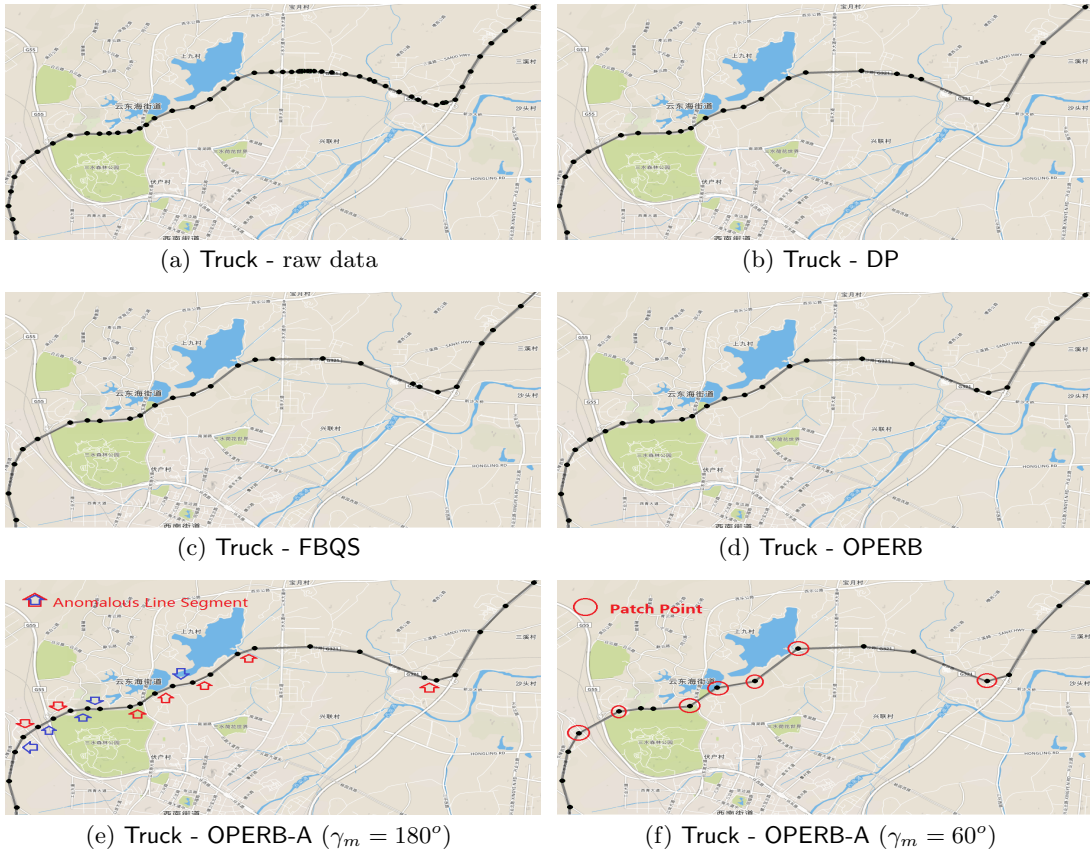


Figure 24: An Example on Truck Trajectories.